How to cite: *Angew. Chem. Int. Ed.* **2024**, *63*, e202406867
doi.org/10.1002/anie.202406867

Analytical Chemistry

Miniaturized Electrochemical Sensing Platforms for Quantitative Monitoring of Glutamate Dynamics in the Central Nervous System

Qi Wang[+], *Chunyu Yang*[+], *Shulin Chen*[+], *and Jinghua Li**

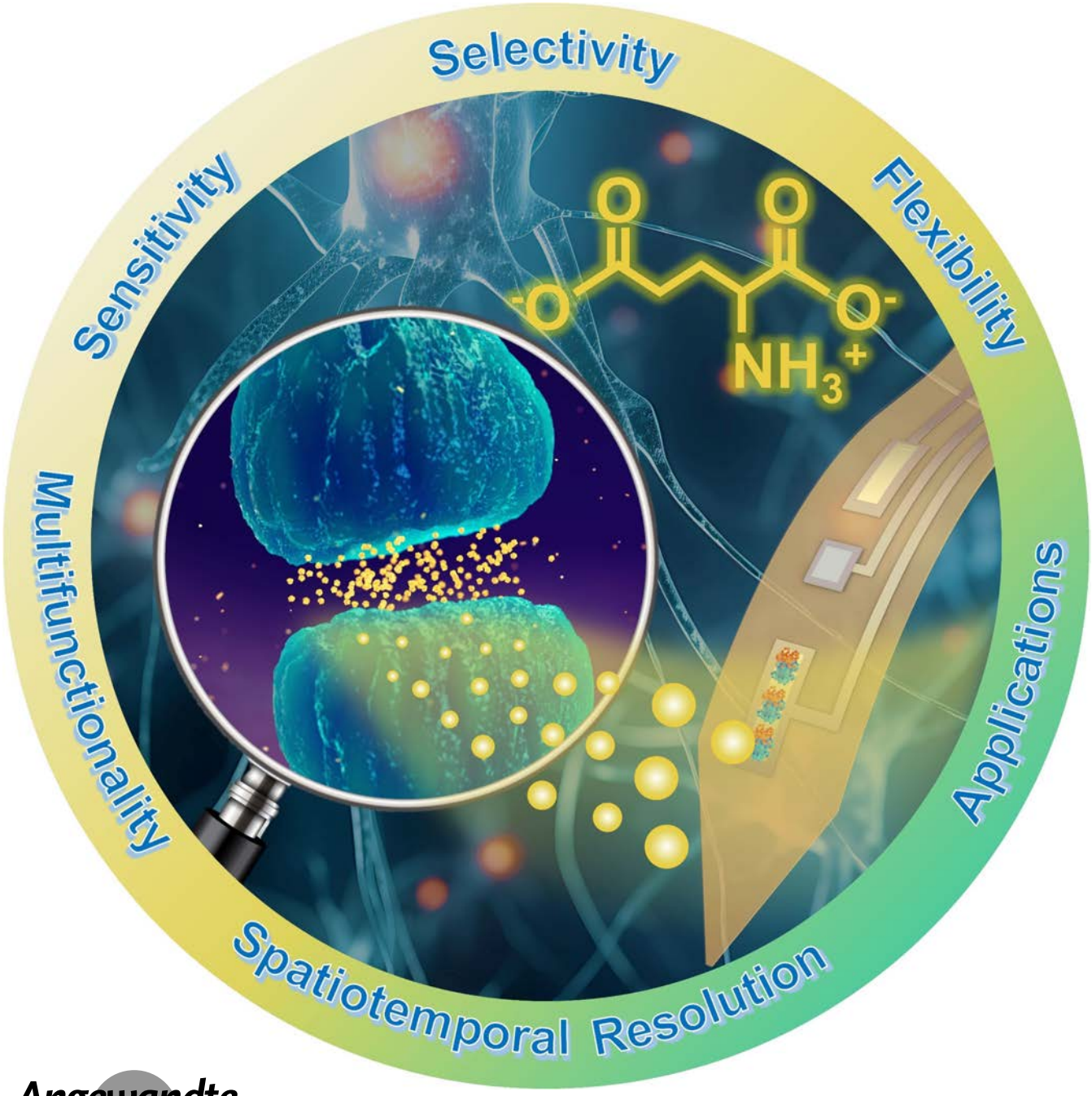

© 2024 The Authors. Angewandte Chemie International Edition published by Wiley-VCH GmbH

Abstract: Glutamate is one of the most important excitatory neurotransmitters within the mammalian central nervous system. The role of glutamate in regulating neural network signaling transmission through both synaptic and extra-synaptic paths highlights the importance of the real-time and continuous monitoring of its concentration and dynamics in living organisms. Progresses in multidisciplinary research have promoted the development of electrochemical glutamate sensors through the co-design of materials, interfaces, electronic devices, and integrated systems. This review summarizes recent works reporting various electrochemical sensor designs and their applicability as miniaturized neural probes to in vivo sensing within biological environments. We start with an overview of the role and physiological significance of glutamate, the metabolic routes, and its presence in various bodily fluids. Next, we discuss the design principles, commonly employed validation models/protocols, and successful demonstrations of multifunctional, compact, and bio-integrated devices in animal models. The final section provides an outlook on the development of the next generation glutamate sensors for neuroscience and neuroengineering, with the aim of offering practical guidance for future research.

1. Introduction

The activities of the central nervous system (CNS) involve numerous biochemical and electrophysiological events occurring in space and time. Among various neuronal chemicals, glutamate is an important excitatory neurotransmitter in the mammalian CNS of particular interest to neuroscientists. It plays an essential role in regulating neural network signaling transmission through both synaptic and extra-synaptic paths. Previous studies have reported that elevated levels of glutamate and glutamate receptor-mediated excitotoxicity are strongly linked to a variety of neurological disorders and diseases.[1–3] In particular, the release of excess glutamate has been found in both human and animals with traumatic brain injury (TBI).[4–7] Due to its correlation with increased neuronal excitability, studies on the release, distribution, and spread of glutamate within living organisms have become a key research area.

Up to now, multiple issues remain yet to be addressed to fully understand the role of glutamate in physiological and pathological pathways. Specifically, as the release of glutamate within the brain is micro-domain specific,[8] techniques that can monitor its concentration with high spatial resolution are desirable. However, how to achieve the accurate, continuous, and real-time quantification of glutamate concentration in localized regions within living systems is still a challenging topic. Conventional sensing techniques, such as microdialysis and glutamate-sensitive fluorescent reporter (iGluSnFR), have drawbacks due to either the limited achievable resolution or the requirement of genetic modification of the target organisms.[9] Moreover, to correlate glutamate release/distribution patterns with other physiological information, such as the neural activities and the concentration of other neuronal chemicals, multifunctional, yet minimally invasive tools are needed for concurrent recording. Recent advancements in biosensing, electrochemistry, and electrical engineering have facilitated the successful development of implantable biosensors that bypass certain of these drawbacks. Nevertheless, the currently available glutamate sensors are still constrained in sensitivity, selectivity, multifunctionality, and minimal invasiveness. In addition, designs that consider the complex environment of CNS and the intrinsic spatiotemporal dynamics of glutamate are necessary to achieve the most accurate results.

This review summarizes design principles and recently reported examples for miniaturized electrochemical glutamate sensors to address these challenges. It begins with an overview of the role of glutamate in the CNS, the corresponding metabolic routes, and its physiologically relevant concentrations in biofluids. A comparison with existing methods highlights the unique opportunities provided by in vivo electrochemical sensors. Next, we explore electrochemical strategies for the accurate quantification of glutamate involving the co-design of recognition elements and signal transduction methods, followed by validation protocols and exemplary applications. Representative works utilizing in vitro, ex vivo, and in vivo models showcase recent efforts and progress in this field. The following section summarizes the advances in creating multifunctional platforms that incorporate glutamate sensing and other modalities, with a focus on the physiological relevance and significance of detecting these signals in conjunction. The conclusion and outlook section provides a perspective on the future directions of glutamate sensor research and applications by emphasizing the synergy of innovations in interfacial materials, electronic devices, integrated systems, and biological models. Together, we aim to provide potential guidelines for building advanced, customizable systems tasked with high performance sensing of glutamate in various locations and scenarios in the CNS.

[*] Q. Wang,[+] C. Yang,[+] S. Chen,[+] Dr. J. Li
Department of Materials Science and Engineering
The Ohio State University
Columbus, OH 43210, USA
E-mail: li.11017@osu.edu

Dr. J. Li
Chronic Brain Injury Program
The Ohio State University
Columbus, OH 43210, USA

[+] These authors contributed equally to this work.

© 2024 The Authors. Angewandte Chemie International Edition published by Wiley-VCH GmbH. This is an open access article under the terms of the Creative Commons Attribution License, which permits use, distribution and reproduction in any medium, provided the original work is properly cited.

15213773, 2024, 34, Downloaded from https://onlinelibrary.wiley.com/doi/10.1002/anie.202406867 by Ohio State University, Wiley Online Library on [12/08/2024]. See the Terms and Conditions (https://onlinelibrary.wiley.com/terms-and-conditions) on Wiley Online Library for rules of use; OA articles are governed by the applicable Creative Commons License

2. The Role of Glutamate in CNS and Its Metabolic Routes

As one of the most important excitatory neurotransmitters, glutamate serves to enhance cognitive functions such as memory and learning. It can facilitate synaptic transmission and plasticity, and its dysregulation is closely related to the development and onset of various neurological and psychiatric disorders. Figure 1a summarizes the metabolism of glutamate involved in the CNS: The glutamate-glutamine (Gln) cycle is the major pathway of glutamate transmission and recycling. During glutamatergic neurotransmission, neurons release glutamate into the extracellular space, followed by the rapid clearance enabled by glial glutamate transporters. The glutamate is then converted to the inert Gln, released to the extracellular fluid (ECF), taken up by neurons, and converted back to glutamate (Figure 1b). To reduce the excitotoxicity, glutamate can be transformed into α-ketoglutarate which can be further metabolized through the tricarboxylic acid (TCA) cycle. Glutamate also serves as a metabolic precursor of γ-aminobutyric acid (GABA)—the primary inhibitory neurotransmitter. The imbalance in cortical excitation/inhibition (E/I) ratio is closely related to the concentrations of glutamate and GABA. The E:I ratio is an important factor in researching numerous neurological disorders.[10–11]

The concentrations of glutamate in bodily fluids are important reference data guiding the design of sensors with compatible working ranges. Within a glutamatergic synapse, the glutaminase catalyzes the synthesis of glutamate in presynaptic neurons from Gln. Consequently, the concentration of glutamate in these neurons is typically higher compared to those in other parts of the synaptic environment. Once released, both presynaptic and postsynaptic neurons as well as astrocytes take up glutamate through excitatory amino acid transporters (EAATs) and other receptors, maintaining synaptic and extracellular glutamate concentrations at homeostatic levels–approximately 10 mM in postsynaptic terminals, around 2 mM in astrocytes,[12] and 0.2–5 μM in the ECF.[13] The concentration also varies according to the health status: it has been reported that glutamate levels in cerebrospinal fluid (CSF) range from 0.1–4.1 μM[14–15] (Figure 1c), but can increase up to 817.9 μM in cases of severe TBI.[16] The protective function of the blood–brain barrier results in a higher concentration of glutamate in other bodily fluids than in the CNS: blood glutamate concentrations span from 25–225 μM,[17] while the value falls between 0–18.4 μM mM^{-1} creatinine in urine[3,18–19] and 14–55.5 μM in saliva.[20–21] Due to differences in the hydration level, glutamate concentration in urine fluctuates significantly compared to in other bodily fluids. Therefore, creatinine, which maintains a relatively stable concentration, is used as a reference to normalize glutamate concentration.[22] On the other hand, there has been no report showing the presence of glutamate in sweat. While the presence of glutamate in the referenced biofluids offers additional opportunities to develop point-of-care systems, further understanding of the physiological significance behind the concentration variation is necessary to use this information as biomarkers for neurological diseases.

The relationship between the dysregulation of glutamate and neurological disorders is complicated and different in specific activities and regions of brain (Figure 1d). An imbalance between excitation and inhibition, specifically involving increased extracellular glutamate, has been identi-

Jinghua Li received her B.S. degree in Biological Sciences from Shandong University, China, in 2011. She earned her Ph.D. from Duke University, United States, in chemistry in 2016. She spent 2016–2019 as a postdoctoral fellow at Northwestern University before joining the Department of Materials Science and Engineering at The Ohio State University as an assistant professor in 2019. Her research interests include biosensing, neural interfaces, and bio-integrated electronics.

Qi Wang received his B.E. and M.S. degrees in Physics from Lanzhou University, China, in 2019 and 2022, respectively. He is currently a Ph.D. student in the Department of Materials Science and Engineering at The Ohio State University, working under the supervision of Dr. Jinghua Li. His research interests include the development of wearable and implantable bioelectronics.

Chunyu Yang received her B.E. in Polymer Science and Engineering from Hubei University and M.S. in Chemistry Engineering and Technology from China University of Petroleum (Beijing), in 2020 and 2023, respectively. She is currently a Ph.D. student in the Department of Materials Science and Engineering at The Ohio State University, working under the supervision of Dr. Jinghua Li. Her research interests lie in wearable, implantable bioelectronics, neural interfaces, and biomedical nanomaterials.

Shulin Chen received her B.E. and M.S. degrees in Biomedical Engineering from Southeast University, China, in 2017 and Northwestern University, United States, in 2019, respectively. Currently she is a Ph.D. candidate studying in Dr. Jinghua Li's group in the Department of Materials Science and Engineering at The Ohio State University. Her current research interests include implantable and wearable bioelectronics.

© 2024 The Authors. Angewandte Chemie International Edition published by Wiley-VCH GmbH

15213773, 2024, 34, Downloaded from https://onlinelibrary.wiley.com/doi/10.1002/anie.202406867 by Ohio State University, Wiley Online Library on [12/08/2024]. See the Terms and Conditions (https://onlinelibrary.wiley.com/terms-and-conditions) on Wiley Online Library for rules of use; OA articles are governed by the applicable Creative Commons License

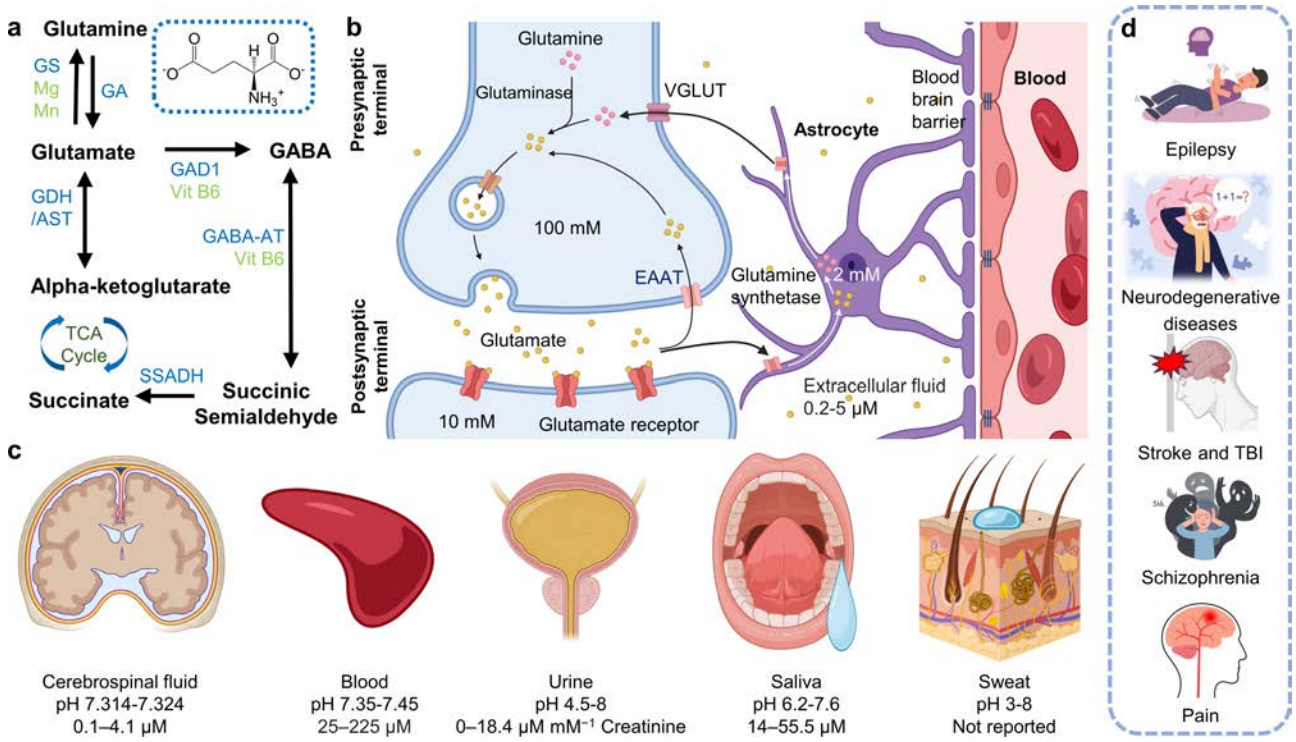

Figure 1. The role of glutamate in the CNS. (a) Schematic diagram of the metabolic pathways involving glutamate and other related neuronal chemicals in the CNS. GS: Gln synthetase, GA: Glutaminase, GAD 1: glutamate decarboxylase, Vit: vitamin, GABA-AT: GABA aminotransferase, SSADH: succinate semialdehyde dehydrogenase, GDH: glutamate dehydrogenase, AST: aspartate transaminase; (b) Compartmentalization of glutamate in CNS; VGLUT: vesicular glutamate transporter; (c) The concentration of glutamate and pH in five main human bodily fluids according to previous reports; (d) Representative neurological and psychiatric disorders linked to dysregulation of glutamate in CNS. Figure created with BioRender.com.

fied as a key factor leading to epilepsy: the majority of previous studies have reported elevated glutamate levels in epileptic regions, although a minority have observed reductions.[23–24] For neurodegenerative diseases like Alzheimer's disease (AD), Amyloid-beta (Aβ) can hinder the efficient uptake of glutamate by astrocytes, which will subsequently initiate a series of destructive processes including neuronal swelling, breakdown of cellular membrane integrity, and, ultimately the cell death.[25–27] During stroke, disruptions in energy metabolism prevent effective glutamate reuptake and lead to its accumulation in the synaptic cleft. Excessive glutamate sustains activation of neuronal receptors, causing an influx of calcium ions into cells. This calcium overload triggers a series of destructive processes and may ultimately extend the impact zone of stroke.[28–29] Evidence from pioneering studies suggests that glutamate dysregulation contributes to the negative symptoms of schizophrenia, as observed by the reduced glutamate levels in the prefrontal regions compared to those in healthy controls.[30] A reduced level of glutamate has been reported in the medial prefrontal cortex (mPFC) in animal models of chronic pain, as the stress-induced release of glucocorticoids may influence glutamate transmission in the mPFC[31] (Figure 1d).

3. Conventional Glutamate Sensing Methods

As a result of the microdomain-specific release[32] and clearing events in the CNS at millisecond scale, the concentration of glutamate near the synaptic cleft fluctuates between nano- to milli-molar.[33–34] The rapid and localized dynamics demand real-time imaging technologies with high spatiotemporal resolution, which, however, remains a daunting challenge in this research field.[34] Among existing technologies, microdialysis is an in vivo sampling strategy for continuous monitoring within localized regions.[35–36] In this method (Figure 2a), a pump delivers artificial cerebrospinal fluid (aCSF) into a probe implanted in specific areas in the CNS at a constant perfusion rate (0.3 to 3 $\mu L\,min^{-1}$).[37] Driven by the concentration gradient, target biomolecules diffuse across a semi-permeable membrane into the probe from the extracellular environment. When coupled to analytical techniques, such as ultra-high performance liquid chromatography-mass spectrometry (UPLC-MS), this method can enable the concurrent detection of multiple neuronal chemicals in a single sample[35] . However, its capability is limited by the time needed for measurement (1–30 min) and large size of the probe (diameter: 220–600 μm). Moreover, multiple factors, such as the concentration and flow rate of aCSF, temperature, and geometry of the membrane, can affect the measurement accuracy. Consequently, microdialysis is usually used to detect variations in analyte concen-

© 2024 The Authors. Angewandte Chemie International Edition published by Wiley-VCH GmbH

15213773, 2024, 34, Downloaded from https://onlinelibrary.wiley.com/doi/10.1002/anie.202406867 by Ohio State University, Wiley Online Library on [12/08/2024]. See the Terms and Conditions (https://onlinelibrary.wiley.com/terms-and-conditions) on Wiley Online Library for rules of use; OA articles are governed by the applicable Creative Commons License

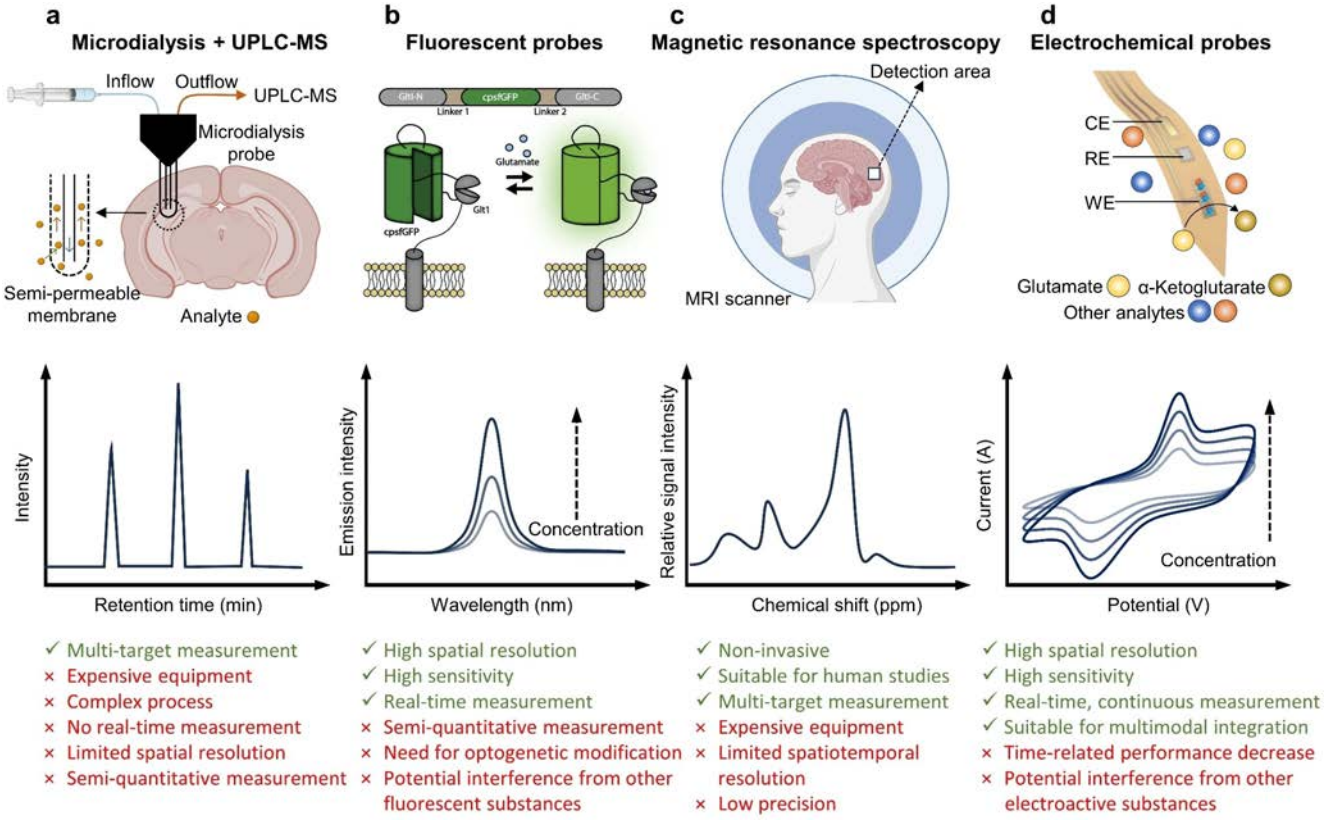

Figure 2. Comparison of existing methods for glutamate sensing, including schematic diagrams, typical data plots, and the advantages and disadvantages of each method. (a) Microdialysis + UPLC-MS, (b) Fluorescent probes, Reproduced from reference [46] with permission. Copyright 2023 Elsevier, (c) MRS and (d) Electrochemical probes. Figure created with BioRender.com.

trations, typically expressed as a percentage of the baseline value[36].

The recently developed glutamate-sensing fluorescence reporter iGluSnFR has been applied in studies of glutamate dynamics in multiple systems and at different scales. Applications span various anatomical sites, such as the retina[38] and olfactory bulb[39] in mice, and visual cortex[40] in cats. Its high spatiotemporal resolution provides opportunities for mesoscale 'functional connectome' mapping[41] and mechanistic studies of a variety of physiological events and disease, including exocytic vesicle fusion,[42] synaptic spillover,[43] cortical spreading depression,[44] and Huntington's disease.[45] iGluSnFR is a single-fluorophore sensor obtained by inserting a circularly permuted green fluorescent protein (cpGFP) into the hinge region of Glutamate transporter I (GltI), part of periplasmic glutamate/aspartate transporter complex from Escherichia coli[46] (Figure 2b). Upon the binding of glutamate, iGluSnFR develops conformational changes in the periplasmic binding protein (PBP) domain, which in turn increases the green fluorescence of cpGFP. This technique demonstrates high sensitivity and high spatiotemporal resolution. By combining the variant SF-Venus-iGluSnFR (Superfolder Venus iGluSnFR) of iGluSnFR with excitation microscopy technology, in vivo imaging of glutamate at kHz level in mouse cortical dendrites has been demonstrated.[47] However, this method requires the genetic modification on target organisms. Engineered protein expression may alter normal neurophysiology, and fluorescent signals are susceptible to interference (e.g., iGluSnFR also responds to aspartate[46]). Additionally, the amount of iGluSnFR may vary widely among individuals depending on factors influencing expression. This issue limits the analysis of glutamate release to semi-quantitative.

Magnetic resonance spectroscopy (MRS) is a non-invasive imaging technology for measuring a wide range of neural metabolites[48] (Figure 2c). Based on the different magnetic resonance frequencies of protons in various substances, MRS can capture the concentrations of multiple chemicals at the same time, including but not limited to choline, creatine (Cr), glutamate, Gln, lactate, lipids, myo-inositol (mIns), and N-acetyl aspartate (NAA).[49] However, because of the limitations of the measurement principle and the magnetic field strength of the instrument, MRS exhibits lower spatial ($0.09–8\ cm^3$)[50–51] and temporal (4.5–45 min)[52–53] resolution. Due to the considerable overlap in the spectrum between different metabolites,[54] measured results require complex data processing. Additionally, the molecular structural similarity between glutamate and Gln results in overlapping signal peaks. Consequently, MRS typically combines them, and the resulting signal is referred to as glutamate + Gln (Glx).[55] These issues result in a

© 2024 The Authors. Angewandte Chemie International Edition published by Wiley-VCH GmbH

15213773, 2024, 34, Downloaded from https://onlinelibrary.wiley.com/doi/10.1002/anie.202406867 by Ohio State University, Wiley Online Library on [12/08/2024]. See the Terms and Conditions (https://onlinelibrary.wiley.com/terms-and-conditions) on Wiley Online Library for rules of use; OA articles are governed by the applicable Creative Commons License

relatively low accuracy of MRS compared with other competing techniques. Electrochemical sensors are an appealing solution to addressing the stated issues and challenges.[56] These probes exploit electrochemical reaction-(s) between a working electrode and glutamate to convert glutamate concentrations into electrical signals (Figure 2d). Recent advances in micro- and nanotechnology have enabled electrochemical devices to be scaled down to probe-type ones with as low as sub-micron dimensions (about 0.5–33 μm)[57–58] for localized or even single-neuron measurements. Pioneering studies have reported high-precision, high-frequency sensing capabilities of electrochemical probes capturing events ranging from ms to s scale (about 0.1 ms–5 s),[57,59] such as the detection of glutamate concentration changes within neural networks or the release signals from individual neuronal exocytosis. Moreover, electrochemical probes can be integrated to form compact, multifunctional bioimplants for simultaneous detection of multiple target substances.[60] However, multiple issues related to the performance and applications, such as the susceptibility to interferents from the surrounding environment, are still worth further exploration. The following sections summarize recent progress and strategies to overcome the limitations.

4. Electrochemical Glutamate Sensing Strategies

Electrochemical sensors convert analyte concentrations into measurable electrical signals through a bioreceptor-functionalized transducer. Glutamate sensing employs a variety of biorecognition elements, including the widely used enzymatic components like glutamate oxidase (GlutOx) and non-enzymatic materials such as metal/metal oxide composites. The enzymatic sensors typically couple with amperometry and galvanic redox potentiometry (GRP), transducing electroactive species associated with the catalysis into electric signals to reflect glutamate concentration change. Non-enzymatic sensors usually work based on direct chemical interactions between glutamate and sensing materials, often requiring specific conditions such as alkaline environments.

Advancements in nucleic acid (i.e., aptamer)-based sensors have enabled improved specificity and sensitivity due to the high affinity between custom designed nucleotide sequences and target analytes. In addition to being used in amperometry, voltammetry, and GRP, these biorecognition elements can also be combined with field-effect transistors (FETs) and organic electrochemical transistors (OECTs) for further improvement in signal quality and detection limit. The intrinsic signal amplification capability of transistors has introduced appealing opportunities for biosensing in complex biological environments. The following section discusses detailed mechanisms and examples.

Figure 3 shows representative strategies employed for glutamate sensing that consider its non-electroactive nature. The classic design utilizes amperometry with a three-electrode setup and measures the Faradaic current at the sensor-solution interface (Figure 3a). By conducting electrochemical reactions of electroactive species associated with the enzymatic/nonenzymatic catalysis of glutamate on the working electrode, amperometry/voltammetry generates a current proportional to the concentration of glutamate which enables quantitative analysis. Amperometric glutamate sensors functionalized with enzymes (e.g., GlutOx,[61–63] glutamate dehydrogenase[64–65]) can be categorized into three generations (Figure 3b): For example, GlutOx catalyzes the following two-electron oxidation reaction: L-glutamate $+ O_2 + H_2O \rightarrow$ α-Ketoglutarate $+ H_2O_2 + NH_3$. The corresponding first-generation biosensors[3] detect electrochemical reactions of electroactive species associated with glutamate oxidation, including O_2 reduction (−0.2 V),[66] H_2O_2 oxidation (0.5 V[66]–0.7 V[67]), or H_2O_2 reduction (−0.5 V).[68] The second-generation design[3] involves redox mediators (e.g., ferricyanide (0.4 V),[69] 6-dichlorophe-nolindophenol (DCIP) (0.1 V)[69–70]) facilitating charge transfer between the enzyme layer and working electrode. Notably, the computer-aided construction of redox mediators shows promise for rapidly screening and optimizing the design to achieve specific goals such as improving electron-tunneling efficiency, enabling low-potential bioelectrocatalysis, reducing competitive inhibition, and enhancing biosensing selectivity.[70] Ferredoxin-dependent glutamate synthase (Fd-GltS),[69–70] an enzyme plays a crucial role in plants, bacteria, and some fungi, demonstrates the capability for bioelectrocatalytic oxidation of glutamate independently of O_2, which is a suitable enzyme for the second-generation sensors. This enzyme operates through a unique mechanism where it directly transfers electrons from glutamate to an electrode via ferredoxin, a small iron-sulfur coenzyme protein, following the chemical reaction as:

$$2\,\text{L-glutamate} + 2\,\text{oxidized ferredoxin} \rightarrow \text{L-glutamine} + \alpha\text{-ketoglutarate} + 2\,\text{reduced ferredoxin} + 2H^+$$

Combined with mediators, this enzyme provides a promising future direction for the development of O_2 independent amperometry glutamate sensors.

The third-generation sensor represents an ideal sensor model where direct electron transfer (DET) occurs between the enzyme and the electrode, without the need for redox mediators. This configuration, if successfully implemented, would offers advantages such as strong interference resistance, rapid response, high sensitivity, and simplicity in device structure. However, as the active sites of biocatalysts used for glutamate sensing (i.e., GlutOx and glutamate dehydrogenase) are deeply embedded within the protein structure and far from the electrode surface, DET is challenging to achieve. To our knowledge, there have not been reports yet of third-generation glutamate sensors so far. Given the similarities in working principles, the potential research directions for third-generation glutamate sensors can be discussed by examining third-generation glucose sensors, although there have been ongoing controversies surrounding them. The core of achieving third-generation sensors lies in maintaining the activity of the enzyme while positioning its active site close to the electrode surface for DET. The main research directions are: 1) Using high-conductivity materials, such as graphene,[71] carbon

© 2024 The Authors. Angewandte Chemie International Edition published by Wiley-VCH GmbH

15213773, 2024, 34, Downloaded from https://onlinelibrary.wiley.com/doi/10.1002/anie.202406867 by Ohio State University, Wiley Online Library on [12/08/2024]. See the Terms and Conditions (https://onlinelibrary.wiley.com/terms-and-conditions) on Wiley Online Library for rules of use; OA articles are governed by the applicable Creative Commons License

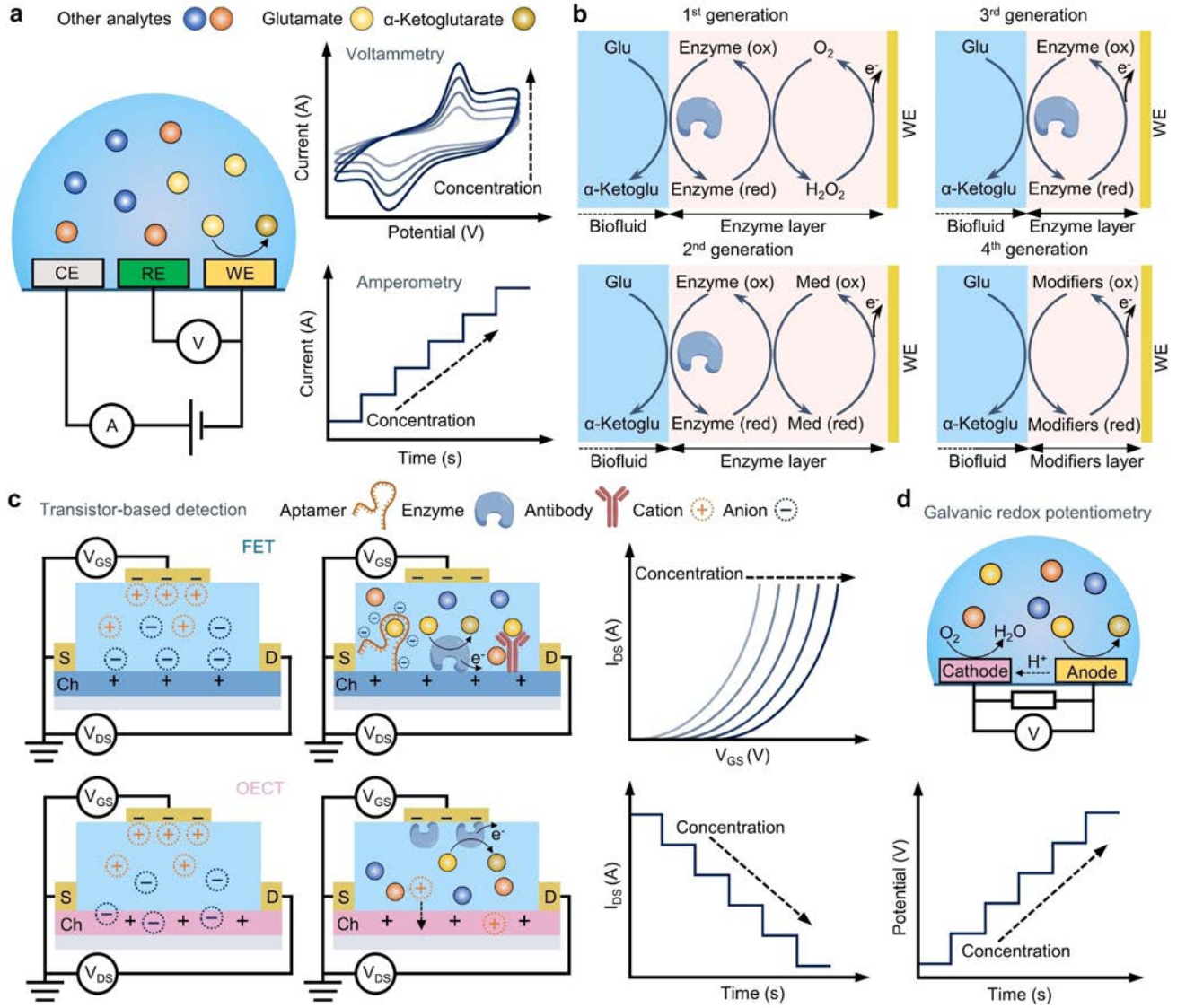

Figure 3. Representative categories of widely employed electrochemical sensing strategies in glutamate detection. (a) Working principle of amperometry/voltammetry and sensor configurations. (b) Schematic illustration of the four generations of amperometric glutamate sensors. (c) Working principles and sensor configurations of transistor-based glutamate sensors including functionalized FETs and OECTs. (d) Working principle of GRP and the corresponding sensor configurations.

nanotubes,[72] and conductive polymers[73] to shorten the distance between the active center of the enzyme and the electrode. 2) Designing functional groups on the electrode surface to immobilize glucose oxidase through self-assembly, shortening the distance between the active center and the electrode, thereby promoting DET efficiency.[74] 3) Reconnstructing oxidoreductase to allow direct contact between the active center and the electrode.[75–77]

Nevertheless, despite existing claims of achieving DET between enzymes and electrodes using these methods, there is a still lack of widely accepted experimental evidence. In reported articles on third-generation sensors, glucose oxidase commonly shows oxidation peaks around −0.4 V, which is considered evidence of DET.[78–80] However, other studies argue that this peak might be due to other factors, such as the adsorption of flavin adenine dinucleotide (FAD):[81] Free FAD, when adsorbed onto glucose oxidase, also shows characteristic peaks around −0.4 V, with the large surface area of nanostructures amplifying this effect. Additionally, nanoparticles similar in size to the enzyme might induce strain in the enzyme protein, potentially causing FAD extrusion.[82] Thus, there is still uncertainty about whether third-generation glucose sensors have been truly achieved.

Alternatively, glutamate detection can be achieved by using non-enzymatic amperometric sensors (sometimes referred to as "the fourth-generation") functionalized with metal/metal oxides.[74,83] This method tends to improve the stability of sensors against changes in environmental factors such as temperature, although at the cost of compromising the specificity due to the lack of biorecognition elements on the working electrode. Besides conventional electrochemical

© 2024 The Authors. Angewandte Chemie International Edition published by Wiley-VCH GmbH

15213773, 2024, 34, Downloaded from https://onlinelibrary.wiley.com/doi/10.1002/anie.202406867 by Ohio State University, Wiley Online Library on [12/08/2024]. See the Terms and Conditions (https://onlinelibrary.wiley.com/terms-and-conditions) on Wiley Online Library for rules of use; OA articles are governed by the applicable Creative Commons License

sensing methods involving the direct catalysis of glutamate, voltammetry utilizing aptamers with redox tags serves as an alternative strategy. Upon target binding, the aptamer undergoes a conformational change, modifying the proximity from the redox reporter to the working electrode, and accordingly, the speed of electron transfer that can be quantified by measuring the Faradaic current. Recent advancements in electrochemistry and microfabrication have allowed for the development of alternative sensing strategies beyond the conventional amperometric Schemes to address the need for improved accuracy and miniaturized form factors. The most widely used examples involve the use of amplification elements, such as FETs[84–85] and OECTs,[63,86] to reduce environmental noise levels (Figure 3c).

In an FET-based glutamate sensor, the biorecognition element is typically immobilized on the semiconductor channel of the transistor. The binding of glutamate to the channel triggers a change in the ion concentration near the channel, leading to a modulation in the local electric field that contributes to the gating of the semiconductor. For example, the enzymatic reaction with GlutOx results in the production of H_2O_2 and NH_3. The conversion of glutamate to NH_3 at the sensor surface leads to a local increase in pH, introducing a negative gating bias voltage.[87] Further dissociation of H_2O_2 may also lead to the generation of H^+ and electrons, as demonstrated in reported glucose sensing systems following a similar mechanism.[88–90]

On the other hand, in an OECT-based sensor working based on the exchange of ions between the electrolyte and semiconductor channel, the biorecognition element, also typically GlutOx, is usually modified on the gate electrode.[91] The catalysis of glutamate generates Faradaic current that alters the voltage drop at the gate-electrolyte interface, changing the effective gate[92] voltage and further modulating the source-drain current as a result of the doping status change of the channel. These transducers can serve as a general platform compatible with multiple bioreceptors, such as antibodies, aptamers, enzymes, and molecularly imprinted polymers.[63,85,93]

One drawback associated with amperometry and voltammetry in monitoring neuronal activity is the concentration gradient and electric field polarization around the recording site.[94] Inspired by the structure of fuel cells, GRP offers a possible solution, as it measures interfacial chemical concentration under thermodynamic equilibrium circumstances (Figure 3d). This design includes an analyte-responsive anode, while the cathode is responsible for the reduction of oxygen. The anodic and cathodic reactions generate an electrical current flow proportional to the concentration of the analytes. Integrating a resistor or a high-impedance voltmeter establishes a potential directly correlated with reactant concentrations at the anode after the system reaches equilibrium. The spontaneous bipolar electrochemistry involved in GRP occurs at conducting objects without external potential polarization, serving as a neuron-compatible strategy for in vivo sensing without impacting firing rates as no external voltage is needed.[95] Through the functionalization of the anode, in vivo measurements of biomarkers such as glutamate (GlutOx),[62] glucose (FAD-GDH),[96] hydrogen sulfide (NiN_4-SAC),[97] and ascorbic acid (SWNTs)[98] have been achieved based on GRP. However, the stability of GRP remains a challenge for in vivo experiments due to the dependence of consistent O_2 level needed for reduction. Some recent works have found a potential way to eliminate the dependence on O_2 by utilizing strategically selected redox molecules such as $K_3Fe(CN)_6$, $Ru(NH_3)_6Cl_3$ and K_2IrCl_6[99–101] as alternative electron acceptors. In this design, the carbon fiber cathode is encapsulated within a glass pipette filled with aCSF containing redox molecules. The positive values ($K_3Fe(CN)_6$: 0.3 V, $Ru(NH_3)_6Cl_3$: 0.1 V, K_2IrCl_6: 0.77 V) of the reduction potential in these molecules entails a high tendency to get reduced in the presence of electron transfer from the anodic indicating electrode. As a result, they can replace the role of O_2, the concentration of which may fluctuate significantly in biological environments. This concept has been successfully demonstrated for the detection of dopamine, ascorbic acid, and serotonin in either one- or two-electrode configuration.[99–101] This concept can potentially be utilized for in vivo glutamate sensing through proper interface design with corresponding recognition elements and redox molecules.

Adopting the signal transduction strategies described above forms various customized sensing platforms for practical applications (Table 1). Figure 4a presents an amperometric sensor configuration involving a GlutOx-functionalized Pt wire (50 μm in diameter) as the working electrode.[61] This sensor innovatively employs a triple-layer structure consisting of ascorbate oxidase, a chitosan matrix, and a selective permeable membrane to mitigate interference from central nervous system compounds, such as ascorbic acid, thereby enhancing the selectivity and anti-interference capability. The outermost layer of ascorbate oxidase eliminates the electroactive ascorbic acid near the sensor, while the chitosan matrix, mixed with GlutOx, further repels ascorbic acid. The innermost selective permeable membrane blocks most large molecular compounds. Another innovation of this sensor is the use of a 50 μm Pt wire. The linear structure and miniaturized form factor of the sensor not only reduce potential damage to biological tissues during implantation and removal but also enable more precise localization for targeting specific brain regions. Figure 4b demonstrates a non-enzymatic glutamate sensor with Ni@nanocarbon (NC) composites prepared by heating the solvothermally synthesized Ni-metal-organic-framework (Ni–MOF) on a glass carbon electrode (3 mm in diameter).[74] The innovation is in achieving non-enzymatic glutamate sensing (fourth-generation glutamate sensor). The sensor is activated in 0.1 M NaOH and measures glutamate through the chemical reaction $NiOOH + \text{glutamate} \rightarrow Ni(OH)_2 + \alpha\text{-ketoglutarate}$ during cyclic voltammetry. One of the advantages of the non-enzymatic sensor is the avoidance of signal instability over time; after 14 days, the peak current remains at 94.7 % of its initial level. However, it is worth noting that metal/metal oxide-based sensors typically require alkaline conditions for operation. This makes them unsuitable for in vivo sensing applications.

© 2024 The Authors. Angewandte Chemie International Edition published by Wiley-VCH GmbH

15213773, 2024, 34, Downloaded from https://onlinelibrary.wiley.com/doi/10.1002/anie.202406867 by Ohio State University, Wiley Online Library on [12/08/2024]. See the Terms and Conditions (https://onlinelibrary.wiley.com/terms-and-conditions) on Wiley Online Library for rules of use; OA articles are governed by the applicable Creative Commons License

Table 1: Summary of representative glutamate sensing strategies reported in the literature and key performance metrics.

Sensing strategy	Working electrode materials	Detection range	Limit of detection	Sensing area	Sensitivity	Response time	Ref
Amperometry	Pt wire/PPD/GlutOx/AsOx	5 to 1.5×10^{2} μM	4.4×10^{-2} μM (reported)	50 μm in diameter	$6.17\times10^{-2}\pm 6.37\times10^{-4}$ μA μM^{-1} mm^{-2}	2.0 s	Ref [61]
Voltammetry—direct method	Ni@NC/GCE	5×10^{-3} to 5×10^{2} μM	1.67×10^{-3} μM (reported)	3 mm in diameter	9.79×10^{-1} μA dec^{-1} mm^{-2}	8.0 s	Ref [74]
Voltammetry—indirect method	Au/Anti glutamate aptamer/MCH	10^{-9} to 10 μM	$1.3\pm0.7\times10^{-9}$ μM (reported)	2 mm in diameter	1.083×10^{-1} μA dec^{-1} mm^{-2}	–	Ref [102]
FET	Au/RGO/PASE/mGluR/BSA	10^{-10} to 10^{-4} μM	10^{-9} μM (reported)	8 μm×100 μm	4.12×10^{-2} μA dec^{-1} mm^{-2}	1.1 s	Ref [84]
OECT	PEDOT: PSS/Pt NPs/GlutOx/BSA	10^{-1} to 10^{3} μM	5 μM (reported)	0.075 cm^2	7.6×10^{-3} μA μM^{-1} mm^{-2}	–	Ref [63]
GRP	Au/CNT/Nafion/GlutOx/BSA	5×10^{1} to 1.2×10^{3} μM	6.9 μM (reported)	50 μm×50 μm	5.1721×10^{-3} mV μM^{-1}	30 s	Ref [62]
Amperometry	Pt/1,3-diaminobenzene (DAB)/GlutOx/BSA	2.2×10^{-1} to 1.5×10^{2} μM	2.20×10^{-1} μM (reported)	150 μm×300 μm	$2.16\times10^{-3}\pm8\times10^{-5}$ μA μM^{-1} mm^{-2}	4.9 s	Ref [103]
OECT	PEDOT: PSS/CNT/PtNPs/Nafion/GlutOx/BSA	10^{-1} to 2×10^{1} μM	10^{-1} μM (reported)	30 μm in diameter, 60 μm in height (cylinder surface)	5.25×10^{1} μA μM^{-1} mm^{-2}	0.1 s	Ref [104]
Amperometry	Pt/PPy/Nafion/GlutOx/BSA	1.68 to 1.09×10^{2} μM	1.68 μM	8.5×10^{-3} mm^2	$2.047\times10^{-3}\pm5.8\times10^{-5}$ μA μM^{-1} mm^{-2}	2.7 ± 0.3 s	Ref [105]
FET	PolySi/Ta_2O_5/TESU/GlutOx/CNBH	10^{-1} to 3.2×10^{2} μM	0.1 μM	100 μm×1 μm	4.5×10^{5} μA dec^{-1} mm^{-2}	-	Ref [87]

* For works not reporting the LOD, the lower limit of the working range is used here.

© 2024 The Authors. Angewandte Chemie International Edition published by Wiley-VCH GmbH

15213773, 2024, 34, Downloaded from https://onlinelibrary.wiley.com/doi/10.1002/anie.202406867 by Ohio State University, Wiley Online Library on [12/08/2024]. See the Terms and Conditions (https://onlinelibrary.wiley.com/terms-and-conditions) on Wiley Online Library for rules of use; OA articles are governed by the applicable Creative Commons License

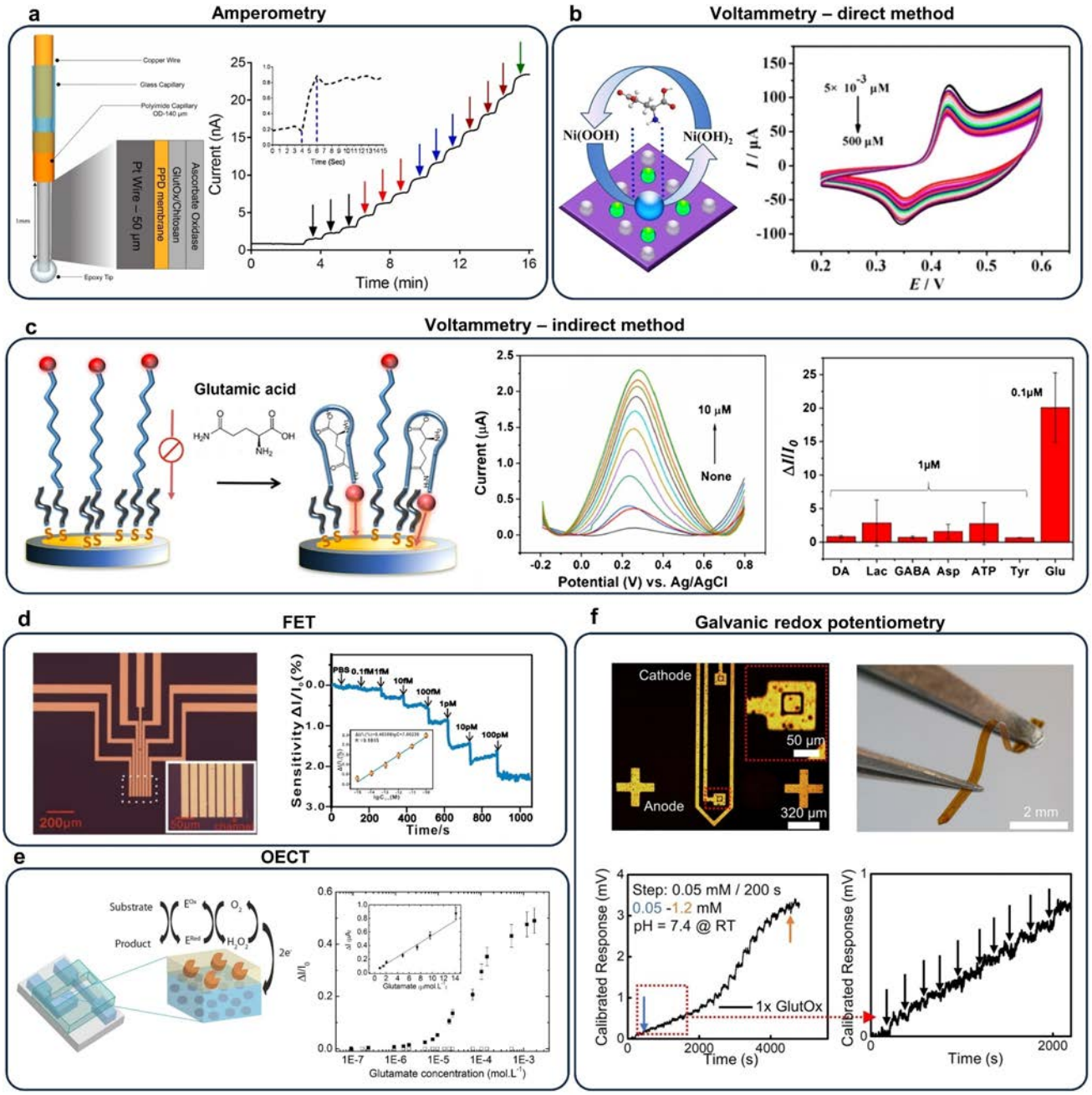

Figure 4. Representative electrochemical glutamate sensors reported in the literature using sensing strategies described in Figure 3. (a) An amperometric glutamate sensor functionalized with AsOx/GlutOx/PPD for measuring glutamate release in rat ventral striatum brain slices and in vivo under electrical stimulation. Reproduced from reference [61] with permission. Copyright 2019 Elsevier. (b) A Ni@NC-Based electrochemical sensor for human urinary glutamate sensing. Reproduced from reference [74] with permission. Copyright 2022 Elsevier. (c) An aptamer functionalized voltammetric sensor for ex vivo glutamate measurements in aCSF and serum, capable of regeneration via hot PBS washing. Reproduced from reference [102] with permission. Copyright 2022 Elsevier. (d) An FET sensor functionalized with reduced RGO for real-time measurement of glutamate release in primary hippocampal neurons. Reproduced from reference [84] with permission. Copyright 2021 Springer Nature. (e) An OECT glutamate sensor functionalized with GlutOx on the gate. Reproduced from reference [63] with permission. Copyright 2023 John Wiley and Sons. (f) An implantable GRP glutamate sensor employing a two-electrode configuration for detecting glutamate release in the hippocampal circuit in mice. Reproduced from reference [62] with permission. Copyright 2023 John Wiley and Sons.

Recent progress in the development of nucleic acid aptamers offers opportunities to further decrease the sensitivity threshold due to the high binding affinity (Figure 4c).[102] Aptamers undergo a conformational change upon specific binding to glutamate, which alters the proximity of the electroactive tags to the electrode surface, converting glutamate concentration into an electrical signal. This mechanism allows the sensor to achieve high selectivity, a low detection limit, and a wide sensing range for glutamate. It also possesses regenerative capabilities, en-

© 2024 The Authors. Angewandte Chemie International Edition published by Wiley-VCH GmbH

15213773, 2024, 34, Downloaded from https://onlinelibrary.wiley.com/doi/10.1002/anie.202406867 by Ohio State University, Wiley Online Library on [12/08/2024]. See the Terms and Conditions (https://onlinelibrary.wiley.com/terms-and-conditions) on Wiley Online Library for rules of use; OA articles are governed by the applicable Creative Commons License

abling continuous detection of glutamate concentrations in aCSF and diluted human serum through hot phosphate-buffered saline (PBS) washing. However, the reversibility and real-time sensing capability of aptamer-based sensors remain to be a challenging aspect compared to their enzyme-based counterparts.

Functionalized transistors have intrinsic signal amplification capability, yielding a high signal-to-noise ratio. Figure 4d presents a reduced graphene oxide (RGO)-based FET sensor with synthesized metabotropic glutamate receptors functionalized on the channel (channel area $\approx$8 μm×100 μm).[84] Due to the high affinity of synthesized metabotropic glutamate receptors for glutamate and the amplification capability of the FET, the sensor achieves an exceptionally low detection limit down to 1 fM. This interface design provides an alternative option to conventional receptors for glutamate for improved sensitivity. Furthermore, the sensor demonstrates excellent biocompatibility and stability, enabling the in situ culture of primary hippocampal neurons on its surface and facilitating the detection of glutamate release induced by high K^+ solution. Similarly, a poly(3,4-ethylenedioxythiophene) polystyrene sulfonate (PEDOT: PSS)-based OECT shown in Figure 4e employs immobilized GlutOx on the gate electrode (0.075 cm^2).[63] This work demonstrates a versatile sensor structure capable of detecting both glutamate and acetylcholine which can be achieved by simply changing the enzyme type on the gate electrode. Spin-coating PEDOT with incorporated platinum nanoparticles as the channel increases the catalytic surface area and enhances the sensitivity. The GlutOx located at the gate oxidizes glutamate, generating a Faradaic current. This process reduces the potential drop between the gate and the electrolyte, thereby increasing the effective gate voltage. Consequently, cations infiltrate the channel, resulting in a decrease in channel conductivity. This general device architecture is potentially applicable to various common enzyme sensing mechanisms based on redox enzymes, enabling the detection of a wide range of target analytes.

Figure 4f demonstrates a flexible, miniaturized sensing probe working based on GRP, with an active working area of as low as 50 μm by 50 μm.[62] This sensor utilizes a simplified two-electrode system: GlutOx catalyzes glutamate oxidation at the anode, while a Pt–C layer on the cathode reduces oxygen. The resulting redox reaction generates a current that is proportional to the concentration of glutamate, which is then converted into voltage across a load resistor. The GRP sensing platform eliminates the use of a potentiostat compared to the conventional three electrode setup for electrochemistry, reduces the complexity, and allows for miniaturization for precise and localized targeting. The sensor exhibits high selectivity against various interferents and successfully demonstrates detection of glutamate release in the hippocampal circuit within mouse brain slices induced by electrical stimulation.

One of the advantages of electrochemical sensors is that they can be integrated to form compact, multifunctional bioimplants for the simultaneous detection of multiple target substances. The overall design principles for sensors detecting alternative biomarkers usually share similar considerations for glutamate sensors that have been discussed in this section. For detailed discussion on the device structures, principles, and design related to simultaneous measurement systems of multiple targets, please refer to Section 6.

5. Validation and Application of Glutamate Sensors in Biological Models

Testing the performance of designed sensing probes requires interfacing them with biotissues and/or neural circuits under physiological conditions, accompanied by release of glutamate triggered by external stimuli. This section summarizes standard methodologies, biological models, and validation protocols commonly used for performance characterization, and exemplary applications based on the resulting systems (Table 2). Existing literature describes two modes of interaction between glutamate and sensing platforms in the time domain. Multiple factors, such as sensor dimensions, sampling rate, and distance from the target, contribute to the two different modes observed experimentally. In the first mode (Figure 5a), sensors with relatively smaller size (0.5–33 μm)[57–58,68,106–107] can capture glutamate release from large unilamellarvesicles (LUVs) or isolated synaptic vesicles at the time scale of 0.1–1 ms.[57–58,68,106–107] This release mode results in time traces showing stochastic bursts of individual sub-ms current spikes corresponding to the rupture of single vesicles at the electrode surface. The spikes display a fast initial rise followed by a slower decay. In a second (also more frequently reported) mode (Figure 5b), sensors (100–500 μm)[59,66,108–113] detect the average level of glutamate overspilled into the extracellular space. The response time is typically in the range of 5 to 500 s[108,113] which corresponds to the period needed for released glutamate to reach the baseplate sensors.

Successful validation depends on robust biological models with well-defined protocols that induce glutamate release across various settings, including in vitro, ex vivo, and in vivo environments. The CNS in rodents serve as viable models due to their structural and functional similarities to that in humans. Neuronal or glial cell cultures provide a highly stable environment for investigating release events such as exocytosis (Figure 5c), where researchers can adjust genetic and external variables for control of experimental parameters.[114–115] Beyond neuronal cultures, acute brain slices offer the advantage of preserving inherent neuronal circuits with well-established synaptic connections and anatomy (Figure 5d). The intact natural synaptic architecture allows for assessment in a consistent way. Acute brain slices also minimize the experimental parameter space needed to evaluate sensing technologies.[116–117] In vivo models, on the other hand, provide a more comprehensive insight for examining the role of glutamate across normal and disease states of the brain[62,113,118–119] (Figure 5e).

Various triggers can induce the stimulation of glutamate release which can be utilized for validation and application purposes. Upon stimulation, neurons undergo Na^+ induced depolarization events. The action potential triggers the

© 2024 The Authors. Angewandte Chemie International Edition published by Wiley-VCH GmbH

15213773, 2024, 34, Downloaded from https://onlinelibrary.wiley.com/doi/10.1002/anie.202406867 by Ohio State University, Wiley Online Library on [12/08/2024]. See the Terms and Conditions (https://onlinelibrary.wiley.com/terms-and-conditions) on Wiley Online Library for rules of use; OA articles are governed by the applicable Creative Commons License

Table 2: Summary of reported glutamate sensing platforms, the corresponding designs/form factors, and the biological models used for performance validation and application.

Application models	Trigger for glutamate release	Stimulation location	Sensing location	Size of probe	Working electrode materials	Ref
Neuronal cultures (hippocampal neuron)	K^+, L-Gln or Zn^{2+}	–	Inside and outside the vesicles	500 nm in diameter 10 μm in length	SiC@C/Pt/GlutOx/PEI/PEDGE	Ref [57]
Brain slices (mouse)	Spontaneous vesicle exocytosis	–	Nucleus accumbens of coronal planes	33 μm in diameter	Carbon fiber/AuNPs/GlutOx	Ref [58]
Brain slices (rat)	Electrical stimulation	Schaffer collateral pathway	CA1 pyramidal layer of hippocampal slices	200 μm in width 125 μm in thickness	Pt/GlutOx/MPD	Ref [110]
Brain slices (mouse)	Optical stimulation	Visual cortex (layer 5)	Visual cortex	500 μm in width	PEDOT:PSS/Carbon platinum/Nafion/GlutOx/BSA	Ref [111]
Brain slices (mouse)	Electrical stimulation (Brain slices)	Primary visual cortex (Brain slices)	Primary visual cortex (Brain slices)	0.25 mm in width 0.25 mm in thickness	$NdNiO_3$/Nafion/GlutOx/BSA	Ref [113]
In vivo (mouse)	Visual stimulation (In vivo)	Eyes (In vivo)	Primary visual cortex (In vivo)	0.30 mm in length		
In vivo (rat)	K^+	Striatum	Striatum	0.144 mm in width 9 mm in length	Ga/Pt/GlutOx/PPD	Ref [112]
In vivo (rat)	Epilepsy model (pilocarpine, diazepam)	Intraperitoneal injection	CA1 region of the hippocampus	0.1 mm in width 0.03 mm in thickness 6 mm in length	Ti/Pt/PtNps/GlutOx/BSA	Ref [59]
In vivo (mouse)	Epilepsy model (kainic acid)	Intraperitoneal injection	Hippocampus	0.1 mm in width 0.03 mm in thickness 3 mm in length	Pt/rGO/GlutOx/BSA	Ref [108]
In vivo (rat, mouse)	Optical stimulation	Left DG region	Right DG region	200 μm in width 125 μm in thickness	Al_2O_3/Pt/GlutOx/MPD	Ref [109]

© 2024 The Authors. Angewandte Chemie International Edition published by Wiley-VCH GmbH

15213773, 2024, 34, Downloaded from https://onlinelibrary.wiley.com/doi/10.1002/anie.202406867 by Ohio State University, Wiley Online Library on [12/08/2024]. See the Terms and Conditions (https://onlinelibrary.wiley.com/terms-and-conditions) on Wiley Online Library for rules of use; OA articles are governed by the applicable Creative Commons License

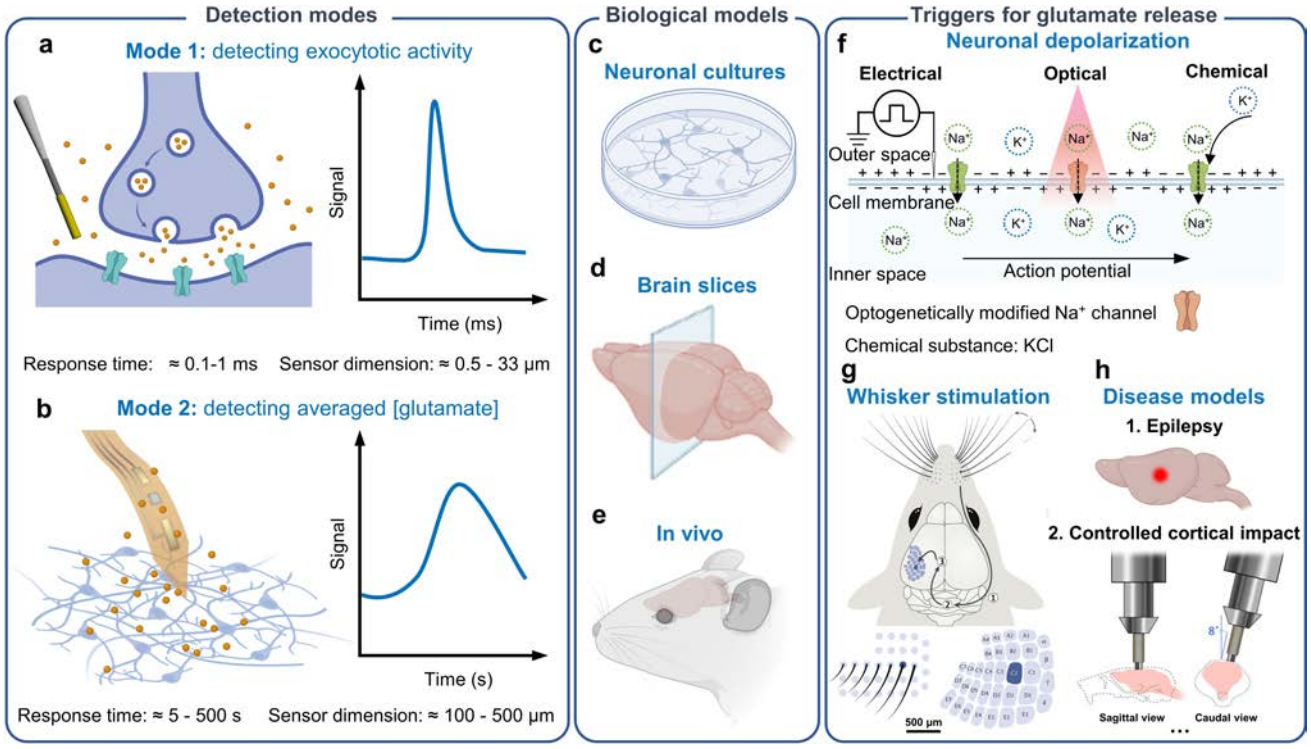

Figure 5. Representative categories of widely employed detection modes, validation models, and triggers utilized for inducing glutamate release. Two detection modes, including (a) detecting exocytotic activity and (b) detecting averaged glutamate concentrations within local domains. The former requires a smaller sensor size (~0.5–33 μm) and has a submillisecond response time (~0.1–1 ms), while the latter requires a larger size (~100–500 μm) and has a second-level response time (~5–500s). Commonly used biological systems for validation and application, including (c) cultured/dissociated neurons, (d) acute brain slices, and (e) in vivo animal models. Main triggers used for inducing glutamate release, including (f) neuronal depolarization (enabled by electrical, optical, chemical stimulation), (g) whisker stimulation. Reproduced from reference [121] with permission. Copyright 2019 Springer Nature, and (h) disease models. Reproduced from reference [127] with permission. Copyright 2007 Elsevier. Figure created with BioRender.com.

opening of voltage-gated calcium channels, resulting in an influx of calcium ions, which in turn stimulates glutamate release from presynaptic terminals through calcium-dependent exocytosis. Reported stimulation strategies include applying electrical pulses,[110] adding KCl[57,112] or optically stimulating genetically modified neurons[109,111] (Figure 5f). Additionally, whiskers are highly sensitive tactile hairs in rodent animals functionally equivalent to human fingertips.[120] Each mystacial whisker on the snout is represented by a large-scale brain structure in the somatosensory cortex, termed a barrel, with organizations similar in rats and mice. Previous studies suggest that touch signals from each whisker evoke sparse patterns of neuronal activity in related primary somatosensory cortex, accompanied by glutamate release through glutamatergic synapses.[121] Consequently, whisker stimulation can assist in examining the role of glutamate in sensory processing, excitatory signaling, and neural plasticity,[122–123] and can also be utilized as a trigger for validating sensor performance (Figure 5g). Furthermore, neurological disorders and controlled cortical impact injury can result in dysregulated glutamate release. Experimentally induced onset of these conditions can serve to upregulate glutamate within the brain. Frequently utilized disease models employed in the literature (although electrochemical sensors may not have been involved yet) include the epilepsy, AD,[124] Parkinson's disease,[125] Schizophrenia,[126] and others. Brain injury models typically involve delivering a mechanical force directly to the exposed dura mater to mimic the biomechanical aspects of TBI, as illustrated in Figure 5h.[121–122]

Following the general protocols outlined in Figure 5, pioneering studies have reported various glutamate sensors, along with validation and/or applications in complex biological environments. Figure 6a demonstrates a chemical vapor deposition-carbon modified SiC (SiC@C) nanowire probe immobilized with Pt/GlutOx (500 nm in diameter and 10 μm in length).[57] The probe serves to measure vesicular glutamate content by intracellular vesicle impact electrochemical cytometry (IVIEC) inside varicosities and the vesicular exocytotic amounts. A series of current spike signals correspond to the exocytotic release from unpaired hippocampal axon varicosities elicited by high-K^+ solution (62.5 mM) puffs. Incubation with Gln (20.5 mM for 15 min) results in a significant increase in vesicular glutamate content and release by approximately 259 % and 183 %, respectively, due to the improvement of glutamate synthesis and intravesicular loading enabled by an increase in Gln concentration. Incubation with Zn^{2+} (100 μM for 180 min) leads to a 42 % decrease in vesicular glutamate content, while increasing the number of released glutamate mole-

© 2024 The Authors. Angewandte Chemie International Edition published by Wiley-VCH GmbH

15213773, 2024, 34, Downloaded from https://onlinelibrary.wiley.com/doi/10.1002/anie.202406867 by Ohio State University, Wiley Online Library on [12/08/2024]. See the Terms and Conditions (https://onlinelibrary.wiley.com/terms-and-conditions) on Wiley Online Library for rules of use; OA articles are governed by the applicable Creative Commons License

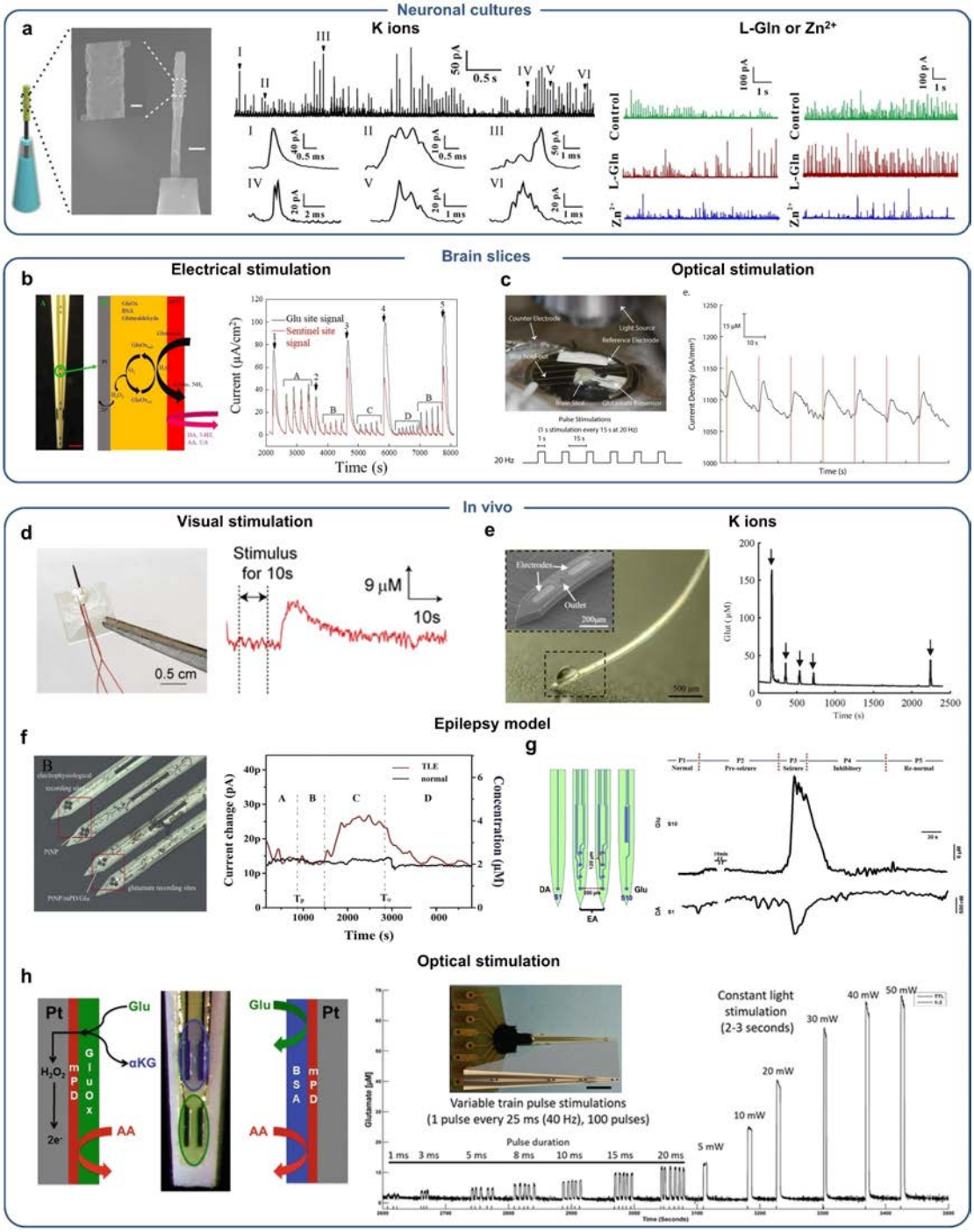

Figure 6. Recently reported, representative electrochemical glutamate sensing platforms together with their demonstrations through in vitro, ex vivo, and in vivo experiments. (a) A Pt/GlutOx modified SiC@C nanowire glutamate probe for monitoring vesicular glutamate release or vesicular glutamate content (scale bars = 1 μm for the main view and 200 nm for the magnified one). Reproduced from reference [57] with permission. Copyright 2021 John Wiley and Sons. (b) A GlutOx/mPD modified probe for measuring glutamate concentration in rat hippocampal slices during electrical stimulation. Reproduced from reference [110] with permission. Copyright 2020 IOP Publishing. (c) A glutamate probe based on GlutOx/Nafion for monitoring glutamate release in primary visual cortex slices during optogenetic stimulation. Reproduced from reference [111] with permission. Copyright 2020 Elsevier. (d) A GlutOx/Nafion-coated perovskite nickel salt glutamate sensor for in vivo monitoring of glutamate release in the mouse visual cortex during visual stimulation. Reproduced from reference [113] with permission. Copyright 2020 Springer Nature. (e) A GlutOx-based probe for monitoring glutamate release in the rat striatum during injection of potassium-enriched artificial cerebrospinal fluid. Reproduced from reference [112] with permission. Copyright 2019 Elsevier. (f) A PtNP and GlutOx-modified probe for detecting hippocampal glutamate concentrations during epileptic seizures in rats. Reproduced from reference [59] with permission. Copyright 2018 Elsevier. (g) A Pt/rGO-modified probe for monitoring glutamate and DA concentrations in the hippocampus during epileptic seizures in rats. Reproduced from reference [108] with permission. Copyright 2019 Elsevier. (h) A GlutOx-modified probe for measuring glutamate release in the DG region of the mouse brain during optogenetic stimulation. Reproduced from reference [109] with permission. Copyright 2018 Springer Nature.

© 2024 The Authors. Angewandte Chemie International Edition published by Wiley-VCH GmbH

15213773, 2024, 34, Downloaded from https://onlinelibrary.wiley.com/doi/10.1002/anie.202406867 by Ohio State University, Wiley Online Library on [12/08/2024]. See the Terms and Conditions (https://onlinelibrary.wiley.com/terms-and-conditions) on Wiley Online Library for rules of use; OA articles are governed by the applicable Creative Commons License

cules by about 33 %. This may be due to the formation of larger final exocytotic pores resulting from Zn^{2+} incubation.

Figure 6b presents a probe capable of in vivo measurement of glutamate concentration in the presence of major interferents (H_2O_2 and AA) (200 μm in width and 125 μm in thickness).[110] The probe has a pair of Pt microelectrodes at the tip. In this strategy, the electrode is modified with GlutOx and m-phenylenediamine (mPD) for detecting glutamate, while the other electrode is only modified with mPD for the quantification of response to the interferent H_2O_2 and AA. The current difference between the two electrodes corresponds to signals sourced from glutamate. The ex vivo validation involves placing the probe into the Cornu Ammonis 1 (CA1) pyramidal layer of rat hippocampal slices followed by providing an electrical stimulation (amplitude: 100 μA, width: 5 ms–1000 ms) in the Schaffer collateral pathway region. Results suggest that the evoked glutamate response scales proportionally with the pulse width.

Figure 6c presents a sensor fabricated using the direct-write printing method for monitoring glutamate release in the visual cortex of mouse brain slice during light stimulation (500 μm in width).[111] Carbon-platinum-PEDOT: PSS composite ink is printed on a flexible substrate, followed by the deposition of a selective permeability membrane Nafion layer and GlutOx. 470 nm blue light illumination triggers the opening of light-gated sodium ion channels, inducing depolarization in pyramid neurons in genetically modified mice. Glutamate is subsequently released and diffuses from the synaptic cleft into sensors at the bottom of the brain slice. Under optical stimulation pulse trains (20 Hz, 5 ms, duration 1 s every 15 s), the sensor detects stable and reproducible glutamate release, with an average concentration of 11.43 ± 2.00 μM. Figure 6d demonstrates an amperometric sensor functionalized with $NdNiO_3$/Nafion for measuring glutamate concentration in the visual cortex of brain slices and awake mice (0.25 mm in width, 0.25 mm in thickness and 10 mm in length).[113] Electrically stimulating layer 4 of the visual cortex in mouse brain slice (500 μA, 0.1 s pulse width, 40 Hz, 5 s duration) leads to glutamate release in layer 2/3 (>21 μM). Afterwards, the sensor is implanted into the binocular region of the primary visual cortex in awake mice, with a continuous 10 s sinusoidal drifting grating provided as the visual stimulus. The sensor detects triggered glutamate rise induced by visual stimulation with a temporal delay higher than the response latency in recorded local field potentials (LFPs) and neuronal spikes. The delay may be attributed to the rapid removal of glutamate from the synaptic cleft and extracellular space by glutamate transport proteins located in presynaptic terminals and astrocytes. As a result, the signal may correspond to excessive glutamate following prolonged stimulation.

Figure 6e presents a temperature-responsive probe with GlutOx. The liquid metal, Ga, serves as both the electrical interconnects and supporting layer at low temperatures (0.144 mm in width and 9 mm in length).[112] The probe can be implanted into the rat brain up to 2 cm deep without the need for external shuttle carriers or coatings in a cooled state. Later, it becomes soft and flexible upon melting of Ga at physiological temperatures. The probe is implanted in the rat striatum, with repeated injections of K^+-rich aCSF (100 mM) serving as the stimulation. Initially, the concentration of glutamate quickly increases and gradually returns to baseline. Subsequent stimulations result in a small amount of glutamate release followed by partial recovery after 25 minutes. A possible reason for this observation is the depletion of readily releasable neuronal glutamate over repetitive stimulation.

Drug administration is a commonly applied strategy for building epilepsy models. For example, injecting kainic acid (an excitatory amino acid receptor agonist) or pilocarpine (a muscarinic acetylcholine receptor agonist) can lead to the onset of acute epileptic seizures, which will be subsequently transitioned to natural recurrent epilepsy. Figure 6f demonstrates a GlutOx-modified probe serving to detect glutamate concentrations in hippocampus of temporal lobe epileptic rats induced by drug (0.1 mm in width, 0.03 mm in thickness and 6 mm in length).[59] After the injection of pilocarpine, the implanted probe monitors the glutamate concentration in the CA1 region of the rat increasing from 2.24 ± 0.35 μM to 4.22 ± 1.07 μM and remaining stable afterwards. The time delay (10 min) may indicate a latency period required for the onset of seizures. The injection of diazepam (an anxiolytic benzodiazepine for terminating epilepsy) suppresses the excessive excitation of the nervous system, causing the glutamate concentration to return to the baseline.

In addition to acute seizures, studies on spontaneous epilepsy can further uncover the complete range of pathophysiological symptoms, signal coupling patterns and underlying pathways. Figure 6g demonstrates a Pt/rGO-modified probe for simultaneous detection of glutamate, dopamine (DA), and electrical signals in the hippocampus during spontaneous epileptic seizures in rats (0.1 mm in width, 0.03 mm in thickness and 3 mm in length).[108] Injecting kainic acid unilaterally into the hippocampus constructs the spontaneous epilepsy model. The probe examines changes in glutamate concentrations together with other biosignals throughout multiple phases during an epileptic seizure: During the normal period, glutamate and DA concentrations remain relatively stable, and neurons discharge normally. In the pre-seizure period, there are increases in glutamate and DA concentrations (2 μM and 300 nM), and neuronal discharge becomes more intense. During the seizure period, glutamate concentration sharply rises (34 μM) while DA concentration decreases (1100 nM), neurons synchronously fire in an intensive release mode, and typical epileptic waves appear. In the inhibitory period, glutamate concentration gradually decreases to normal levels, while DA concentration rises to normal levels, and neuronal discharge is significantly inhibited. In the re-normal period, electrophysiological activity gradually returns to normal.

Figure 6h shows a GlutOx-modified probe for measuring glutamate release in the dentate gyrus (DG) region of the mouse brain during optogenetic stimulation (200 μm in width and 125 μm in thickness).[109] Genetic modification introduces the expression of the light-sensitive protein

© 2024 The Authors. Angewandte Chemie International Edition published by Wiley-VCH GmbH

15213773, 2024, 34, Downloaded from https://onlinelibrary.wiley.com/doi/10.1002/anie.202406867 by Ohio State University, Wiley Online Library on [12/08/2024]. See the Terms and Conditions (https://onlinelibrary.wiley.com/terms-and-conditions) on Wiley Online Library for rules of use; OA articles are governed by the applicable Creative Commons License

Channelrhodopsin-2 (ChR2) in the right DG region. Afterwards, light pulse trains serve as the stimulation (power: 0.5 mW, frequency: 20 Hz, duration: 2.5 s). Increasing the pulse width from 1 ms to 20 ms results in a linear increase in the peak concentration of glutamate. Continuous light stimulation (2–3 s) with an increasing power (5 mW to 50 mW) leads to a gradual increase and then stabilization of peak concentration. One possible reason is the limit posed by the maximum light dispersion of blue light (488 nm) within the brain. Together, the exemplary neural probes and associated validations/applications serve as successful demonstrations for the design and characterization of glutamate sensing in mammalian CNS systems.

6. Simultaneous Recording of Glutamate Concentration and Other Biochemical/Electrophysiological Signals

The functioning of the brain, as well as the pathology of neurological diseases and neurotrauma, involve coupling among various neurotransmitters and electrophysiological processes. Due to the key role of glutamate in synaptic transmission and network activity in the CNS and its correlation with increased neuronal excitability, simultaneous monitoring of its concentration together with other biomarkers and/or biosignals can provide insights into physiological and pathological pathways. This section summarizes recent works on multifunctional sensing platforms incorporating glutamate sensors for concurrent monitoring of spatially resolved biological events within microdomains (Table 3).

The imbalance of cortical E/I ratio is related to various neurological disorders including seizures, trauma, and autism spectrum disorders. Glutamate and GABA are the most abundant excitatory and inhibitory neurotransmitters, respectively. Their physiological significance has inspired research on the development of probes for their simultaneous detection.[118–119,128] Figure 7a[129] presents a dual functional glutamate-GABA sensor. GABase catalyzes the conversion of GABA (in the presence of α-ketoglutarate) to glutamate for further detection using GlutOx. The system consists of five 50 μm×100 μm electrodes: The central one serves for pseudo-referencing to provide the baseline, with two on right side for the detection of glutamate and GABA. The two on the left side function as self-referencing for these neurotransmitters. Specifically, since the GABA sensor has both GlutOx and GABase, it records signals from both glutamate and GABA. Thus, the signal from the glutamate sensor needs to be subtracted from the GABA sensor data to obtain the concentration of GABA. In vivo tests of the dual glutamate:GABA sensor in the cortical layer 4 of the primary barrel cortex of the rat demonstrates consistent signal increases for both neurotransmitters (11.98 μM for glutamate and 29.63 μM for GABA) upon stimulation with KCl.

Designing sensor arrays that can measure both glutamate concentration and electrophysiology in a defined brain region is also of great interest, which can provide mechanistic insights into how the glutamate spread in the extracellular space impacts neural network excitability.[130–131] Recently, adopting this concept has offered various customized multifunctional platforms for measurement in various brain regions including striatum,[132] hippocampus,[53] from cortex to thalamus,[133] and from cortex to hippocampus.[134–135] Figure 7b[8] shows such a dual-mode implantable microelectrode array (IMEA) that records action potentials, LFPs and glutamate concentration. The IMEAs are designed to have four probes (7 and 9 mm in length and 100 μm in width), which allow for simultaneous detection in the cortex and hippocampus of rats through a 2 mm differential. The 16 electrodes (12 and 17 μm in diameter) are tailored for concurrent glutamate sensing and electrophysiological measurements with minimized brain tissue impact. In vivo studies using epileptic rats reveal that a buildup of glutamate concentration, particularly in the hippocampus, precedes abnormal, violent bursts of electrophysiological signals induced by pilocarpine. Light-activated ruthenium-bipyridine-triphenylphosphine-γ-aminobutyric acid (RuBi-GABA) suppresses the dual-mode signals due to the induced release of GABA for inhibition. Those results suggest that the change in hippocampal glutamate levels is closely coupled to electrophysiology and thereby, can serve as biomarkers for epileptic activity.

Ascorbate acts as an antioxidant, enzyme co-factor, and modulator of energetic metabolism, glutamate signaling, and nitric oxide-dependent pathways. Previous works have reported that fluctuations in extracellular glutamate and ascorbate levels are coupled through a hetero-exchange mechanism.[136] Both glutamate and ascorbate correlate with neurodegenerative diseases such as Alzheimer's and Huntington's. Figure 7c[136] shows a study combining carbon fiber microelectrodes and ceramic-based microelectrode arrays for the detection of ascorbate and glutamate, respectively. Recording basal ascorbate levels in the CA1, CA3, and DG sub-regions of the hippocampus in rats suggests region-specific modulation. Simultaneous recordings in the CA1 subregion indicate a dynamic correlation of ascorbate levels peaking at the end of the glutamate peak. Successive square wave voltammograms validate that the amperometric signal measured corresponds to ascorbate.

Both DA and glutamate in the striatum can influence motor coordination, motivated behavior, and reward-seeking activities. Their ability to reciprocally modulate the release and reuptake of each other suggests the importance of concurrent recording in understanding their combined influence on striatal function. Figure 7d[137] shows a design of glutamate sensors by encapsulating GlutOx within an electrodeposited chitosan hydrogel matrix. This technique employs fast-scan cyclic voltammetry (FSCV) to simultaneously quantify glutamate and DA at single location, a feature unachievable with traditional fixed-potential amperometry. Placing the sensor at discrete locations in the ventral striatum of acute rat brain slices successfully measures the release of glutamate and DA in response to a biphasic electrical stimulus. Perfusing the slices with glutamine (metabolic precursor to glutamate) and dl-threo-β-benzylox-

© 2024 The Authors. Angewandte Chemie International Edition published by Wiley-VCH GmbH

15213773, 2024, 34, Downloaded from https://onlinelibrary.wiley.com/doi/10.1002/anie.202406867 by Ohio State University, Wiley Online Library on [12/08/2024]. See the Terms and Conditions (https://onlinelibrary.wiley.com/terms-and-conditions) on Wiley Online Library for rules of use; OA articles are governed by the applicable Creative Commons License

Table 3: Summary of recently reported multifunctional neural probes incorporating glutamate sensors for simultaneous detection of biochemical and electrophysiological signals that are relevant to the study of neurological diseases and brain functions.

Simultaneously recorded signals	Relevant diseases and/or brain functions mentioned in the work	Detection range reported in the work	Size of probe	Trigger	Sensing location	Ref
GABA	Seizures, trauma, and autism spectrum disorder	GABA: 10–100μM; glutamate: 5–100 μM	495 μm in width, 125 μm in thickness	KCl	Cortical layer 4 of primary barrel cortex of rat	Ref [129]
GABA	Seizures and autism	GABA: 0–2200μM; glutamate: 0–1200 μM	127 μm in diameter; 10 mm in length	Monophasic electrical stimulus	CA1 region of the hippocampus of rat	Ref [118]
GABA	Epilepsy, depression, schizophrenia, and drug abuse	GABA: 0–100 μM; glutamate: –	–	KCl	Frontal cortex, motor cortex and dorsal striatum of rat	Ref [119]
Electrophysiology	Epilepsy	Glutamate: 0.3–68 μM	Four probes, two with 7 mm in length, another with 9 mm in length, 100 μm in width	Pilocarpine and RuBi-GABA	Cortex and hippocampus of rat	Ref [8]
Electrophysiology	Hippocampus function	Glutamate:0.56–100 μM	4 shafts with 85 μm spacing, 100 μm in width, 30 μm in thickness and 6 mm in length	–	CA1, DG and CA3 of hippocampus of rat	Ref [135]
Electrophysiology	Epilepsy	Glutamate: 0–50 μM	4 shafts with 200 μm spacing, 100 μm in width,30 μm in thickness and 6 mm in length	Pilocarpine and diazepam	CA1 of hippocampus of rat	Ref [59]
Electrophysiology	Parkinson's disease, stroke, and epilepsy	Glutamate: 5–30 μM	7 mm in length, 30 μm ×343 μm in cross section	KCl	Striatum of rat	Ref [132]
Electrophysiology	Epilepsy	Glutamate: 0–50 μM	4 shafts with 200 μm spacing, 100 μm in width,30 μm in thickness and 6 mm in length	–	Cortex and hippocampus of mice	Ref [104]
Electrophysiology	Hippocampus function	Glutamate: 5–30 μM	4 shafts with 200 μm spacing, 100 μm in width,30 μm in thickness and 6 mm in length	–	Cortex and hippocampus of mice	Ref [134]
Electrophysiology	Brain death	Glutamate: 5–25 μM	7 mm in length, 30 μm in thickness, 343 μm in width	KCl	Striatum of rat	Ref [138]
Multiple neurochemicals and electrophysiology	Parkinson's disease and schizophrenia	Lactate and glucose: 500–8000 μM; glutamate: 5–80 μM; choline:10–150 μM	144 μm in width, 40 μm in thickness, 3.06 mm and 4.09 mm in length	KCl	Hippocampus, mPFC and MD region of mice	Ref [60]
Ascorbate	Alzheimer's or Huntington's disease	Glutamate: 5–1600 μM; ascorbate: –	Ascorbate sensor: 50 μm in diameter, 150–250 μm in length; glutamate sensor: 200 μm in width, 50 μm in thickness, 1.2 mm in length	KCl and glutamate	CA1, CA3, and DG of the hippocampus of rat	Ref [136]
DA	Striatal function	Glutamate: 0–500 μM; DA: 0–1000 μM	30 μm in diameter,100 μm in length	Biphasic electrical stimulus	Ventral striatum of acute rat brain slices	Ref [137]

© 2024 The Authors. Angewandte Chemie International Edition published by Wiley-VCH GmbH

15213773, 2024, 34, Downloaded from https://onlinelibrary.wiley.com/doi/10.1002/anie.202406867 by Ohio State University, Wiley Online Library on [12/08/2024]. See the Terms and Conditions (https://onlinelibrary.wiley.com/terms-and-conditions) on Wiley Online Library for rules of use; OA articles are governed by the applicable Creative Commons License

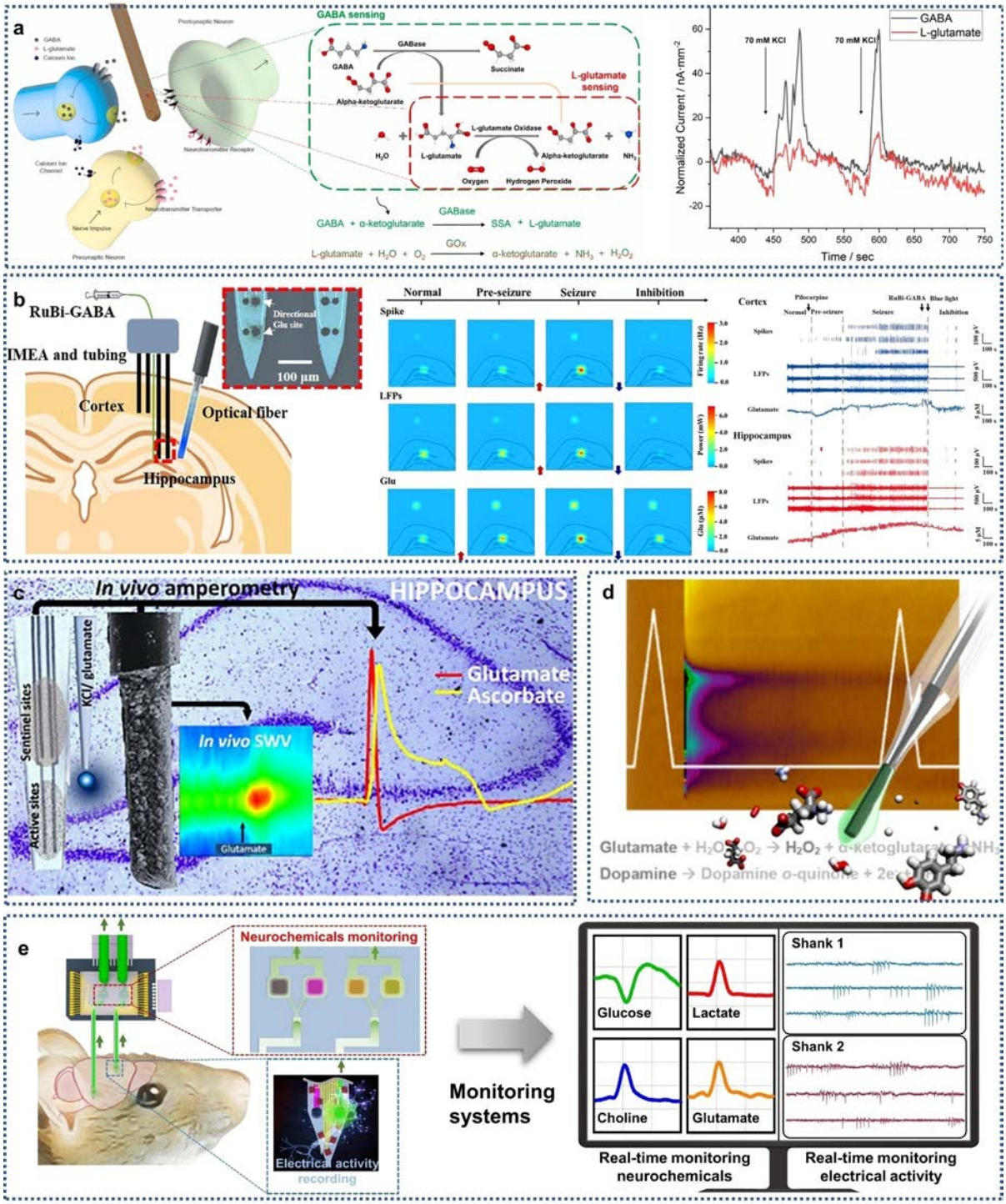

Figure 7. Examples of compact and minimally invasive neural probes for simultaneous, multimodal recording of glutamate and other related physiological signals. (a) A dual L-glutamate:GABA sensor that detects neurotransmitters in extracellular space via enzymatic reactions, with α-ketoglutarate for the GABase reaction supplied by the L-glutamate oxidation. Reproduced from reference [129] with permission. Copyright 2023 Elsevier. (b) Dual-mode microelectrode arrays tracking the electrophysiology and glutamate levels in the cortex and hippocampus of epileptic rats, along with the heat map of spike firing rate, LFP power, and glutamate concentration during seizure and inhibition period. Reproduced from reference [8] with permission. Copyright 2023 American Chemical Society. (c) Carbon fiber nanocomposite sensors and ceramic microbiosensor arrays concurrently measuring ascorbate and glutamate in hippocampus sub-regions of anesthetized rats. Reproduced from reference [136] with permission. Copyright 2018 Elsevier. (d) FSCV with a carbon-fiber microbiosensor for simultaneous, real-time detection of glutamate and DA in the striatum of rat brain slices at a single location. Reproduced from reference [137] with permission. Copyright 2018 Elsevier. (e) A RTBM neural probe equipped with integrated biosensors for the concurrent tracking of multiple neurochemicals and electrical neural activity by channeling ECF to the biosensors for immediate concentration analysis. Reproduced from reference [60] with permission. Copyright 2024 National Academy of Sciences.

© 2024 The Authors. Angewandte Chemie International Edition published by Wiley-VCH GmbH

15213773, 2024, 34, Downloaded from https://onlinelibrary.wiley.com/doi/10.1002/anie.202406867 by Ohio State University, Wiley Online Library on [12/08/2024]. See the Terms and Conditions (https://onlinelibrary.wiley.com/terms-and-conditions) on Wiley Online Library for rules of use; OA articles are governed by the applicable Creative Commons License

yaspartic acid (dl-TBOA) (potent inhibitor of the EAATs) results in a significant increase in glutamate concentration and a modest one in DA concentration. The results may demonstrate the role of glutamate in potentiating DA release.

Dyskinesia in Parkinson's disease correlates with changes in various neurotransmitters like serotonin, GABA, and glutamate. Similarly, schizophrenia is characterized by abnormal neurotransmission across multiple brain regions like mesocortical, mesolimbic, and prefrontal-hippocampal circuits. Figure 7e[60] demonstrates a real-time bimodal (RTBM) neural probe that concurrently measures four neurochemicals including glucose, lactate, choline, and glutamate and electrical activity in various brain regions including hippocampus, mPFC, and mediodorsal thalamus (MD). To prevent crosstalk of different chemicals, a polydimethylsiloxane (PDMS)-based microfluidic chip is integrated, which delivers ECF to dedicated biosensors located in individual chambers. This design also allows for mixing multiple drugs for potential chemical stimulation in future applications. The RTBM neural probe implanted into the hippocampus of mouse detects significant increases in neuronal firing rates and subsequent neurochemical changes following KCl injection, including a decrease in glucose concentration and increases in lactate, choline, and glutamate concentrations. The probe also detects activities in both the mPFC and MD regions following KCl stimulation to the mPFC. Results suggest that some neurons in the MD region are functionally connected to mPFC neurons through a glutamatergic pathway.

7. Conclusion and Outlook

This review has summarized recent advances in development of electrochemical sensors for glutamate sensing, with particular attention to their usage as compact, bio-integrated electronics for in vivo applications within the CNS. While multiple designs have been reported, GlutOx-functionalized amperometric sensors remain to be the predominant category because of the overall consideration of sensitivity, selectivity, robustness, reliability, and reversibility. However, the stability of such sensors represents an unresolved issue due to the fast degradation speed of enzymes in biological environments, which can cause rapid decreases in electrical performance as well as baseline drift after implantation. As a result, most glutamate sensors are designed for acute usage only, although they could play important roles in assessing the progression of chronic neurotrauma and neurodegenerative diseases. Two strategies can potentially resolve this issue: first, using surface passivation materials to extend the lifespan, and second, introducing mathematical model-based ongoing calibration processes at regular intervals to ensure accurate functionality over time (in a way like the continuous glucose monitors in the market).

Another concern is with the mismatch between physiologically relevant concentrations of glutamate in biofluids and the working range of sensors (which is related to both the capacities of the bioreceptors and transducers). While most reported sensors can detect a portion of the concentration of glutamate in the CNS, many fall short in capturing subtle changes in the ambient glutamate levels, which serve as an important measure of pathological conditions. To this end, integrating on-chip thin-film amplifiers, such as FETs and OECTs, through microfabrication can minimize the influence of environmental noises and improve the limit of detection and quantification. However, the complexity increases when considering that the response of the sensor is typically not linear across the entire concentration span. Addressing this issue requires developing mathematical models for calibration that can be applied throughout the entire working range of sensors. Variations among devices and organisms add additional complications in determining baseline readings. Consequently, while calculating the change in glutamate concentration is feasible, precisely determining the absolute concentrations represents a greater hurdle.

Despite progress in improving the spatial resolution enabled by micro- and nanofabrication, how to achieve high temporal resolution to reveal glutamate dynamics in vivo is another issue. As stated earlier, the synaptic event of glutamate release and uptake occurs rapidly at a sub-ms scale. Observing excessive activation of glutamate receptors and the associated dynamic patterns may inform the process of excitotoxicity underlying neurological diseases. Nevertheless, most current studies report the average level of glutamate concentration within larger microdomains as a result of the overspill of excessive glutamate into the extracellular space after clearance, with slow response times measured at the scale of seconds. Tackling this challenge requires a synergy of strategies, including using a higher sampling rate, developing miniaturized probes for improved interface with synapses, and enhancing the response speed between bioreceptors and glutamate—whichever is the bottleneck constraining the temporal resolution. FSCV may offer additional strength, but the diffusion and chemical reaction time needed for signal transduction remain to be limiting factors. It is essential to address this issue such that electrochemical sensing strategies can be competitive when compared with iGluSnFR for imaging ms scale glutamate dynamics.

Efforts are also needed to build advanced multifunctional systems for establishing biometric signature profiles. This demand is essential not only because of the physiological relevance/significance to study the coupling of these signals in space and time, but also the need for precise calibration of glutamate sensing itself: Many works to date focus on improving the performance of sensors first and then demonstrating applications in animal studies, but sophisticated, dynamic physiological events occurring concurrently in the background and their impacts are often overlooked. As one example out of many, significant shifts in local pH and oxygen concentrations may occur when synaptic terminals are activated. This will add interferences to the interpretation of glutamate sensing data.

Finally, beyond the sensing modality, advanced neuroengineering should incorporate the closed-loop management functionality by involving modulation capacity as well.

© 2024 The Authors. Angewandte Chemie International Edition published by Wiley-VCH GmbH

15213773, 2024, 34, Downloaded from https://onlinelibrary.wiley.com/doi/10.1002/anie.202406867 by Ohio State University, Wiley Online Library on [12/08/2024]. See the Terms and Conditions (https://onlinelibrary.wiley.com/terms-and-conditions) on Wiley Online Library for rules of use; OA articles are governed by the applicable Creative Commons License

Further integration of electrical/optical stimulation and/or drug delivery systems will provide desired modalities for targeted interventions in response to real-time neuronal chemical fluctuation. Overall, further addressing these challenges in in vivo glutamate sensing can offer simple, compact, and minimally invasive methods, which can contribute to diagnostics and treatments for improving the prognosis and quality of life for patients with neurological diseases.

Acknowledgements

This work was supported by The Ohio State University start-up funds, the Chronic Brain Injury Pilot Award Program at The Ohio State University, and National Science Foundation award ECCS-2223387. This work was also supported by the Ohio State University Materials Research Seed Grant Program, funded by the Center for Emergent Materials; NSF-MRSEC, grant DMR-2011876; the Center for Exploration of Novel Complex Materials; and the Institute for Materials and Manufacturing Research.

Conflict of Interest

The authors declare no conflict of interest.

Data Availability Statement

Data sharing is not applicable to this article as no new data were created or analyzed in this study.

Keywords: Glutamate · Biosensing · Bio-integrated Electronics · Neural Interfaces · Electrochemistry

[1] C. Baliatsas, J. Bolte, J. Yzermans, G. Kelfkens, M. Hooiveld, E. Lebret, I. V. Kamp, *Int. J. Hyg. Environ. Health* **2015**, *218*, 331–344.
[2] M. Cruz-Haces, J. Tang, G. Acosta, J. Fernandez, R. Shi, *Transl. Neurodegener.* **2017**, *6*, 1–10.
[3] J. Schultz, Z. Uddin, G. Singh, M. M. R. Howlader, *Analyst* **2020**, *145*, 321–347.
[4] A. Zauner, R. Bullock, A. J. Kuta, J. Woodward, H. F. Young, *Act. Neur. S.* **1996**, *67*, 40–44.
[5] L. Shutter, K. A. Tong, B. A. Holshouser, *J. Neurotrauma* **2004**, *21*, 1693–1705.
[6] R. Bullock, A. Zauner, J. J. Woodward, J. Myseros, S. C. Choi, J. D. Ward, A. Marmarou, H. F. Young, *J. Neurosurg.* **1998**, *89*, 507–518.
[7] A. I. Faden, P. Demediuk, S. S. Panter, R. Vink, *Science* **1989**, *244*, 798–800.
[8] J. Xie, Y. Dai, Y. Xing, Y. Wang, G. Yang, E. He, Z. Xu, P. Fan, F. Mo, Y. Wu, Y. Song, X. Cai, *ACS Sens.* **2023**, *8*, 1810–1818.
[9] J. S. Marvin, B. Scholl, D. E. Wilson, K. Podgorski, A. Kazemipour, J. A. Müller, S. Schoch, F. J. Urra Quiroz, N. Rebola, H. Bao, J. P. Little, A. N. Tkachuk, E. Cai, A. W. Hantman, S. S. H. Wang, V. J. DePiero, B. G. Borghuis, E. R. Chapman, D. Dietrich, D. A. DiGregorio, D. Fitzpatrick, L. L. Looge, *Nat. Methods* **2018**, *15*, 936–939.
[10] H. Bruining, R. Hardstone, E. L. Juarez-Martinez, J. Sprengers, A. E. Avramiea, S. Simpraga, S. J. Houtman, S. S. Poil, E. Dallares, S. Palva, B. Oranje, J. M. Palva, H. D. Mansvelder, K. Linkenkaer-Hansen, *Sci. Rep.* **2020**, *10*, 9195.
[11] S. Kirischuk, *Int. J. Mol. Sci.* **2022**, *23*, 5746.
[12] M. Nedergaard, T. Takano, A. J. Hansen, *Nat. Rev. Neurosci.* **2002**, *3*, 748–755.
[13] Q. R. Smith, *J. Nutr.* **2000**, *130*, 1016S–1022S.
[14] M. Peres, E. Zukerman, C. S. Soares, E. Alonso, B. Santos, M. Faulhaber, *Cephalalgia* **2004**, *24*, 735–739.
[15] J. F. Stover, K. Lowitzsch, O. S. Kempski, *Neurosci. Lett.* **1997**, *238*, 25–28.
[16] J. I. M. Brown, A. J. Baker, S. J. Konasiewicz, R. J. Moulton, *J. Neurotrauma* **1998**, *15*, 253–263.
[17] W. Bai, W. L. Zhu, Y. L. Ning, P. Li, Y. Zhao, N. Yang, X. Chen, Y. L. Jiang, W. Q. Yang, D. P. Jiang, L. Y. Chen, Y. G. Zhou, *Sci. Rep.* **2017**, *7*, 5380.
[18] C. G. Bailey, R. M. Ryan, A. D. Thoeng, C. Ng, K. King, J. M. Vanslambrouck, C. Auray-Blais, R. J. Vandenberg, S. Bröer, J. E. Rasko, *J. Clin. Invest.* **2011**, *121*, 446–453.
[19] A. Scinska-Bienkowska, E. Wrobel, D. Turzynska, A. Bidzinski, E. Jezewska, H. Sienkiewicz-Jarosz, K. Golembiowska, W. Kostowski, A. Kukwa, A. Plaznik, P. Bienkowski, *Nutr. Neurosci.* **2006**, *9*, 25–31.
[20] S. Ogawa, J. Takiguchi, M. Shimizu, K. Nako, M. Okamura, Y. Kinouchi, S. Ito, *Tohoku J. Exp. Med.* **2016**, *239*, 103–110.
[21] A. Shimada, B. E. Cairns, N. Vad, K. Ulriksen, A. M. L. Pedersen, P. Svensson, L. Baad-Hansen, *J. Headache Pain* **2013**, *14*, 1–9.
[22] S. S. Waikar, V. S. Sabbisetti, J. V. Bonventre, *Kidney Int.* **2010**, *78*, 486–494.
[23] G. L. Sarlo, K. F. Holton, *Seizure* **2021**, *91*, 213–227.
[24] M. Erecińska, I. A. Silver, *Prog. Neurobiol.* **1990**, *35*, 245–296.
[25] M. E. Conway, *Biogerontology* **2020**, *21*, 257–274.
[26] N. Fayed, P. J. Modrego, G. Rojas-Salinas, K. Aguilar, *Am. J. Alzheimers Dis. Other Demen.* **2011**, *26*, 450–456.
[27] R. Rupsingh, M. Borrie, M. Smith, J. Wells, R. Bartha, *Neurobiol. Aging* **2011**, *32*, 802–810.
[28] D. B. Kirdajova, J. Kriska, J. Tureckova, M. Anderova, *Front. Cell. Neurosci.* **2020**, *14*, 51.
[29] S. Passlick, C. R. Rose, G. C. Petzold, C. Henneberger, *Front. Cell. Neurosci.* **2021**, *15*, 637784.
[30] A. Marsman, M. P. Van Den Heuvel, D. W. Klomp, R. S. Kahn, P. R. Luijten, H. E. H. Pol, *Schizophr. Bull.* **2013**, *39*, 120–129.
[31] B. Naylor, N. Hesam-Shariati, S. Boag, T. Newton-John, C. D. Rae, S. M. Gustin, *Front. Neurol.* **2019**, *10*, 460034.
[32] D. Xie, C. Song, T. Qin, Z. Zhai, J. Cai, J. Dai, T. Sun, Y. Xu, *Sci. Rep.* **2023**, *13*, 18586.
[33] J. D. Clements, R. A. J. Lester, G. Tong, C. E. Jahr, G. L. Westbrook, *Science* **1992**, *258*, 1498–1501.
[34] J. Day-Cooney, R. Dalangin, H. Zhong, T. Mao, *J. Neurochem.* **2023**, *164*, 284–308.
[35] J. Bongaerts, D. D. Bundel, D. Mangelings, I. Smolders, Y. V. Heyden, A. V. Eeckhaut, *J. Pharm. Biomed. Anal.* **2018**, *161*, 192–205.
[36] S. Parrot, L. Denoroy, *Biochemical Approaches for Glutamatergic Neurotransmission*, Humana Press, New York **2018**, pp. 431–467.
[37] V. I. Chefer, A. C. Thompson, A. Zapata, T. S. Shippenberg, *Curr. Protoc. Neurosci.* **2009**, *47*, 7–1.
[38] S. J. Park, I. J. Kim, L. L. Looger, J. B. Demb, B. G. Borghuis, *J. Neurosci.* **2014**, *34*, 3976–3981.
[39] D. Brunert, Y. Tsuno, M. Rothermel, M. T. Shipley, M. Wachowiak, *J. Neurosci.* **2016**, *36*, 6820–6835.

© 2024 The Authors. Angewandte Chemie International Edition published by Wiley-VCH GmbH

15213773, 2024, 34, Downloaded from https://onlinelibrary.wiley.com/doi/10.1002/anie.202406867 by Ohio State University, Wiley Online Library on [12/08/2024]. See the Terms and Conditions (https://onlinelibrary.wiley.com/terms-and-conditions) on Wiley Online Library for rules of use; OA articles are governed by the applicable Creative Commons License

[40] P. O'Herron, P. Y. Chhatbar, M. Levy, Z. Shen, A. E. Schramm, Z. Lu, P. Kara, *Nature* **2016**, *534*, 378–382.
[41] Y. Xie, A. W. Chan, A. McGirr, S. Xue, D. Xiao, H. Zeng, T. H. Murphy, *J. Neurosci.* **2016**, *36*, 1261–1272.
[42] H. Bao, M. Goldschen-Ohm, P. Jeggle, B. Chanda, J. M. Edwardson, E. R. Chapman, *Nat. Struct. Mol. Biol.* **2016**, *23*, 67–73.
[43] J. M. Rosa, R. Bos, G. S. Sack, C. Fortuny, A. Agarwal, D. E. Bergles, J. G. Flannery, M. B. Feller, *eLife* **2015**, *4*, e09590.
[44] R. Enger, W. Tang, G. F. Vindedal, V. Jensen, P. Johannes Helm, R. Sprengel, L. L. Looger, E. A. Nagelhus, *Cereb. Cortex* **2015**, *25*, 4469–4476.
[45] R. Jiang, B. Diaz-Castro, L. L. Looger, B. S. Khakh, *J. Neurosci.* **2016**, *36*, 3453–3470.
[46] J. S. Marvin, B. G. Borghuis, L. Tian, J. Cichon, M. T. Harnett, J. Akerboom, A. Gordus, S. L. Renninger, T. W. Chen, C. I. Bargmann, M. B. Orger, E. R. Schreiter, J. B. Demb, W. B. Gan, S. A. Hires, L. L. Looger, *Nat. Methods* **2013**, *10*, 162–170.
[47] A. Kazemipour, O. Novak, D. Flickinger, J. S. Marvin, A. S. Abdelfattah, J. King, P. M. Borden, J. J. Kim, S. H. Al-Abdullatif, P. E. Deal, E. W. Miller, E. R. Schreiter, S. Druckmann, K. Svoboda, L. L. Looger, K. Podgorski, *Nat. Methods* **2019**, *16*, 778–786.
[48] D. Pasanta, J. L. He, T. Ford, G. Oeltzschner, D. J. Lythgoe, N. A. Puts, *Neurosci. Biobehav. Rev.* **2023**, *144*, 104940.
[49] M. G. Saleh, R. A. Edden, L. Chang, T. Ernst, *Magn. Reson. Med.* **2020**, *84*, 2312–2326.
[50] D. Xu, A. P. Chen, C. Cunningham, J. A. Osorio, S. J. Nelson, D. B. Vigneron, *Magn. Reson. Imaging* **2006**, *24*, 69–74.
[51] I. B. Ip, H. Bridge, *Brain Struct. Funct.* **2022**, *227*, 1491–1505.
[52] L. An, M. F. Araneta, C. Johnson, J. Shen, *Magn. Reson. Med.* **2018**, *80*, 1776–1786.
[53] P. G. Antuono, J. L. Jones, Y. Wang, S. J. Li, *Neurology* **2001**, *56*, 737–742.
[54] H. H. Lee, H. Kim, *Magn. Reson. Med.* **2019**, *82*, 33–48.
[55] I. Pavlova, J. Ruda-Kucerova, *Prog. Neuro-Psychopharmacol. Biol. Psychiatry* **2023**, 110808.
[56] C. Hu, L. Wang, S. Liu, X. Sheng, L. Yin, *ACS Nano* **2024**, *18*, 3969–3995.
[57] X. K. Yang, F. L. Zhang, W. T. Wu, Y. Tang, J. Yan, Y. L. Liu, C. Amatore, W. H. Huang, *Angew. Chem.* **2021**, *133*, 15937–15942.
[58] Y. Wang, D. Mishra, J. Bergman, J. D. Keighron, K. P. Skibicka, A. S. Cans, *ACS Chem. Neurosci.* **2019**, *10*, 1744–1752.
[59] Z. Li, Y. Song, G. Xiao, F. Gao, S. Xu, M. Wang, Y. Zhang, F. Guo, J. Liu, Y. Xia, *Anal. Biochem.* **2018**, *550*, 123–131.
[60] U. Chae, J. Woo, Y. Cho, J. K. Han, S. H. Yang, E. Yang, H. Shin, H. Kim, H. Y. Yu, C. J. Lee, I. J. Cho, *Proc. Nat. Acad. Sci.* **2023**, *120*, e2219231120.
[61] M. Ganesana, E. Trikantzopoulos, Y. Maniar, S. T. Lee, B. J. Venton, *Biosens. Bioelectron.* **2019**, *130*, 103–109.
[62] P. Nithianandam, T. L. Liu, S. Chen, Y. Jia, Y. Dong, M. Saul, A. Tedeschi, W. Sun, J. Li, *Angew. Chem. Int. Ed.* **2023**, *62*, e202310245.
[63] L. Kergoat, B. Piro, D. T. Simon, M. C. Pham, V. Noël, M. Berggren, *Adv. Mater.* **2014**, *26*, 5658–5664.
[64] Y. Matos-Peralta, M. Antuch, D. G. Abradelo, L. Bazán-Bravo, K. R. D. L. L. Hernández, *J. Electrochem. Soc.* **2019**, *166*, B1146.
[65] B. Liang, S. Zhang, Q. Lang, J. Song, L. Han, A. Liu, *Anal. Chim. Acta* **2015**, *884*, 83–89.
[66] T. N. H. Nguyen, J. K. Nolan, H. Park, S. Lam, M. Fattah, J. C. Page, H. E. Joe, M. B. G. Jun, H. Lee, S. J. Kim, R. Shi, H. Lee, *Biosens. Bioelectron.* **2019**, *131*, 257–266.
[67] J. J. Burmeister, V. A. Davis, J. E. Quintero, F. Pomerleau, P. Huettl, G. A. Gerhardt, *ACS Chem. Neurosci.* **2013**, *4*, 721–728.
[68] Y. Wang, H. Fathali, D. Mishra, T. Olsson, J. D. Keighron, K. P. Skibicka, A. S. Cans, *J. Am. Chem. Soc.* **2019**, *141*, 17507–17511.
[69] F. Wu, P. Yu, X. Yang, Z. Han, M. Wang, L. Mao, *J. Am. Chem. Soc.* **2018**, *140*, 12700–12704.
[70] Z. Han, F. Wu, P. Yu, L. Mao, *Anal. Chem.* **2022**, *94*, 8033–8040.
[71] B. Unnikrishnan, S. Palanisamy, S. M. Chen, *Biosens. Bioelectron.* **2013**, *39*, 70–75.
[72] W. C. Wu, J. L. Huang, Y. C. Tsai, *Mater. Sci. Eng. C* **2012**, *32*, 983–987.
[73] M. Zhao, X. Wu, C. Cai, *J. Phys. Chem. C* **2009**, *113*, 4987–4996.
[74] Y. Xu, T. Zhu, Y. Niu, B. C. Ye, *Microchem. J.* **2022**, *175*, 107229.
[75] M. Şenel, C. Nergiz, M. Dervisevic, E. Çevik, *Electroanalysis* **2013**, *25*, 1194–1200.
[76] M. Şenel, M. Dervisevic, E. Çevik, *Curr. Appl. Phys.* **2013**, *13*, 1199–1204.
[77] I. Willner, V. Heleg-Shabtai, R. Blonder, E. Katz, G. Tao, A. F. Bückmann, A. Heller, *J. Am. Chem. Soc.* **1996**, *118*, 10321–10322.
[78] B. Kowalewska, K. Jakubow, *Sens. Actuators B* **2017**, *238*, 852–861.
[79] Z. Kang, K. Jiao, C. Yu, J. Dong, R. Peng, Z. Hu, S. Jiao, *RSC Adv.* **2017**, *7*, 4572–4579.
[80] X. Zhong, W. Yuan, Y. Kang, J. Xie, F. Hu, C. M. Li, *ChemElectroChem* **2016**, *3*, 144–151.
[81] P. N. Bartlett, F. A. Al-Lolage, *J. Electroanal. Chem.* **2018**, *819*, 26–37.
[82] G. S. Wilson, *Biosens. Bioelectron.* **2016**, *82*, vii–viii.
[83] M. Y. Ali, D. Knight, M. M. Howlader, *Biosensors* **2023**, *13*, 237.
[84] Y. T. Li, X. Jin, L. Tang, W. L. Lv, M. M. Xiao, Z. Y. Zhang, C. Gao, G. J. Zhang, *Anal. Chem.* **2019**, *91*, 8229–8236.
[85] N. K. Singh, P. D. Thungon, P. Estrela, P. Goswami, *Biosens. Bioelectron.* **2019**, *123*, 30–35.
[86] K. Xie, N. Wang, X. Lin, Z. Wang, X. Zhao, P. Fang, H. Yue, J. Kim, J. Luo, S. Cui, F. Yan, P. Shi, *eLife* **2020**, *9*, e50345.
[87] D. Braeken, D. Rand, A. Andrei, R. Huys, M. Spira, S. Yitzchaik, J. Shappir, G. Borghs, G. Callewaert, C. Bartic, *Biosens. Bioelectron.* **2009**, *24*, 2384–2389.
[88] Y. Zhu, Q. Wei, Q. Jin, G. Li, Q. Zhang, H. Xiao, T. Li, F. Wei, Y. Luo, *Nanomaterials* **2023**, *13*, 604.
[89] B. Wang, Y. Luo, L. Gao, B. Liu, G. Duan, *Biosens. Bioelectron.* **2021**, *171*, 112736.
[90] Q. Liu, Y. Liu, F. Wu, X. Cao, Z. Li, M. Alharbi, A. N. Abbas, M. R. Amer, C. Zhou, *ACS Nano* **2018**, *12*, 1170–1178.
[91] J. Liao, H. Si, X. Zhang, S. Lin, *Sensors* **2019**, *19*, 218.
[92] Y. Yao, W. Huang, J. Chen, X. Liu, L. Bai, W. Chen, Y. Cheng, J. Ping, T. J. Marks, A. Facchetti, *Adv. Mater.* **2023**, *35*, 2209906.
[93] A. Dudina, U. Frey, A. Hierlemann, *Sensors* **2019**, *19*, 3080.
[94] C. Xu, F. Wu, P. Yu, L. Mao, *ACS Sens.* **2019**, *4*, 3102–3118.
[95] F. Wu, P. Yu, L. Mao, *Chem. Soc. Rev.* **2017**, *46*, 2692–2704.
[96] J. Lu, X. Zhuang, H. Wei, R. Liu, W. Ji, P. Yu, W. Ma, L. Mao, *Anal. Chem.* **2024**, *96*, 3672–3678.
[97] C. Pan, F. Wu, J. Mao, W. Wu, G. Zhao, W. Ji, W. Ma, P. Yu, L. Mao, *J. Am. Chem. Soc.* **2022**, *144*, 14678–14686.
[98] H. Wei, L. Li, J. Jin, F. Wu, P. Yu, F. Ma, L. Mao, *Anal. Chem.* **2020**, *92*, 10177–10182.
[99] P. Yu, H. Wei, P. Zhong, Y. Xue, F. Wu, Y. Liu, J. Fei, L. Mao, *Angew. Chem. Int. Ed.* **2020**, *59*, 22652–22658.

© 2024 The Authors. Angewandte Chemie International Edition published by Wiley-VCH GmbH

15213773, 2024, 34, Downloaded from https://onlinelibrary.wiley.com/doi/10.1002/anie.202406867 by Ohio State University, Wiley Online Library on [12/08/2024]. See the Terms and Conditions (https://onlinelibrary.wiley.com/terms-and-conditions) on Wiley Online Library for rules of use; OA articles are governed by the applicable Creative Commons License

[100] H. Wei, L. Li, Y. Xue, P. Yu, L. Mao, *Anal. Chem.* **2023**, *95*, 8232–8238.
[101] F. Zhu, Y. Xue, W. Ji, X. Li, W. Ma, P. Yu, Y. Jiang, L. Mao, *Angew. Chem. Int. Ed.* **2023**, *62*, e202212458.
[102] C. Wu, D. Barkova, N. Komarova, A. Offenhäusser, M. Andrianova, Z. Hu, A. Kuznetsov, D. Mayer, *Anal. Bioanal. Chem.* **2022**, *414*, 1609–1622.
[103] A. Weltin, J. Kieninger, B. Enderle, A. K. Gellner, B. Fritsch, G. A. Urban, *Biosens. Bioelectron.* **2014**, *61*, 192–199.
[104] X. Wu, J. Feng, J. Deng, Z. Cui, L. Wang, S. Xie, C. Chen, C. Tang, Z. Han, H. Yu, X. Sun, H. Peng, *Sci. China Chem.* **2020**, *63*, 1281–1288.
[105] L. N. Q. Hoa, H. R. Chen, T. T. C. Tseng, *Electroanalysis* **2018**, *30*, 561–570.
[106] Q. F. Qiu, F. L. Zhang, Y. Tang, X. W. Zhang, H. Jiang, Y. L. Liu, W. H. Huang, *Electroanalysis* **2018**, *30*, 1054–1059.
[107] X. K. Yang, F. L. Zhang, X. K. Jin, Y. T. Jiao, X. W. Zhang, Y. L. Liu, C. Amatore, W. H. Huang, *Proc. Natl. Acad. Sci. USA* **2023**, *120*, e2219994120.
[108] G. Xiao, S. Xu, Y. Song, Y. Zhang, Z. Li, F. Gao, J. Xie, L. Sha, Q. Xu, Y. Shen, X. Cai, *Sens. Actuators B* **2019**, *288*, 601–610.
[109] J. J. Burmeister, *Biochemical Approaches for Glutamatergic Neurotransmission*, Humana Press, New York **2018**, pp. 327–351.
[110] C. Tan, P. T. Doughty, K. Magee, T. A. Murray, S. Siddiqui, P. U. Arumugam, *J. Electrochem. Soc.* **2020**, *167*, 027528.
[111] T. N. Nguyen, J. K. Nolan, X. Cheng, H. Park, Y. Wang, S. Lam, H. Lee, S. J. Kim, R. Shi, A. A. Chubykin, H. Lee, *J. Electroanal. Chem.* **2020**, *866*, 114136.
[112] X. Wen, B. Wang, S. Huang, M. S. Lee, P. S. Chung, Y. T. Chow, I. W. Huang, H. G. Monbouquette, N. T. Maidment, P. Y. Chiou, *Biosens. Bioelectron.* **2019**, *131*, 37–45.
[113] Y. Sun, T. N. H. Nguyen, A. Anderson, X. Cheng, T. E. Gage, J. Lim, Z. Zhang, H. Zhou, F. Rodolakis, Z. Zhang, I. Arslan, S. Ramanathan, H. Lee, A. A. Chubykin, *ACS Appl. Mater. Interfaces* **2020**, *12*, 24564–24574.
[114] T. Rajarathinam, D. Thirumalai, S. Jayaraman, S. Yang, A. Ishigami, J. H. Yoon, H. j Paik, J. Lee, S. C. Chang, *Int. J. Biol. Macromol.* **2024**, *254*, 127903.
[115] T. Qian, H. Wang, P. Wang, L. Geng, L. Mei, T. Osakada, L. Wang, Y. Tang, A. Kania, V. Grinevich, R. Stoop, D. Lin, M. Luo, Y. Li, *Nat. Biotechnol.* **2023**, *41*, 944–957.
[116] S. Cho, A. Wood, M. R. Bowlby, *Curr. Neuropharmacol.* **2007**, *5*, 19–33.
[117] E. H. Chang, S. T. Carreiro, S. A. Frattini, P. T. Huerta, *Bioelectron. Med.* **2019**, *5*, 1–12.
[118] P. T. Doughty, I. Hossain, C. Gong, K. A. Ponder, S. Pati, P. U. Arumugam, T. A. Murray, *Sci. Rep.* **2020**, *10*, 12777.
[119] J. J. Burmeister, D. A. Price, F. Pomerleau, P. Huettl, J. E. Quintero, G. A. Gerhardt, *J. Neurosci. Methods* **2020**, *329*, 108435.
[120] J. Lu, B. Chen, M. Levy, P. Xu, B. X. Han, J. Takatoh, P. Thompson, Z. He, V. Prevosto, F. Wang, *Sci. Adv.* **2022**, *8*, eabn6530.
[121] C. C. H. Petersen, *Nat. Rev. Neurosci.* **2019**, *20*, 533–546.
[122] M. Adibi, *Front. Syst. Neurosci.* **2019**, *13*, 40.
[123] J. Fernández-Montoya, C. Avendaño, P. Negredo, *Int. J. Mol. Sci.* **2017**, *19*, 69.
[124] J. V. Andersen, S. K. Christensen, E. W. Westi, M. Diaz-delCastillo, H. Tanila, A. Schousboe, B. I. Aldana, H. S. Waagepetersen, *Neurobiol. Dis.* **2021**, *148*, 105198.
[125] Y. Zhang, X. Meng, Z. Jiao, Y. Liu, X. Zhang, S. Qu, *ACS Chem. Neurosci.* **2020**, *11*, 406–417.
[126] D. Inta, H. Monyer, R. Sprengel, A. Meyer-Lindenberg, P. Gass, *Neurosci. Biobehav. Rev.* **2010**, *34*, 285–294.
[127] G. Onyszchuk, B. Al-Hafez, Y. Y. He, M. Bilgen, N. E. J. Berman, W. M. Brooks, *J. Neurosci. Methods.* **2007**, *160*, 187–196.
[128] N. Moldovan, I. I. Blaga, S. Billa, I. Hossain, C. Gong, C. E. Jones, T. A. Murray, R. Divan, S. Siddiqui, P. U. Arumugam, *Sens. Actuators B* **2021**, *337*, 129795.
[129] S. S. Chu, H. A. Nguyen, D. Lin, M. Bhatti, C. E. Jones-Tinsley, A. H. Do, R. D. Frostig, Z. Nenadic, X. Xu, M. M. Lim, H. Cao, *Biosens. Bioelectron.* **2023**, *222*, 114941.
[130] E. A. Matthews, W. Sun, S. M. McMahon, M. Doengi, L. Halka, S. Anders, J. A. Mueller, P. Steinlein, N. S. Vana, G. V. Dyk, J. Pitsch, A. J. Becker, A. Pfeifer, E. T. Kavalali, A. Lamprecht, C. Henneberger, V. Stein, S. Schoch, D. Dietrich, *Cereb. Cortex* **2022**, *32*, 3669–3689.
[131] K. Zheng, D. A. Rusakov, *Biophys. J.* **2015**, *108*, 2457–2464.
[132] W. Wei, Y. Song, L. Wang, S. Zhang, J. Luo, S. Xu, X. Cai, *Microsyst. Nanoeng.* **2015**, *1*, 1–6.
[133] G. Xiao, Y. Zhang, S. Xu, Y. Song, Y. Dai, X. Li, J. Xie, Y. Wang, Y. Xing, X. Cai, *Sens. Actuators B* **2020**, *317*, 128137.
[134] X. Fan, Y. Song, Y. Ma, S. Zhang, G. Xiao, L. Yang, H. Xu, D. Zhang, X. Cai, *Sensors* **2016**, *17*, 61.
[135] G. Xiao, Y. Song, S. Zhang, L. Yang, S. Xu, Y. Zhang, H. Xu, F. Gao, Z. Li, X. Cai, *J. Neurosci. Methods* **2017**, *291*, 122–130.
[136] N. R. Ferreira, A. Ledo, J. Laranjinha, G. A. Gerhardt, R. M. Barbosa, *Bioelectrochemistry* **2018**, *121*, 142–150.
[137] L. C. Kimble, J. S. Twiddy, J. M. Berger, A. G. Forderhase, G. S. McCarty, J. Meitzen, L. A. Sombers, *ACS Sens.* **2023**, *8*, 4091–4100.
[138] W. Wei, Y. Song, X. Fan, S. Zhang, L. Wang, S. Xu, X. Ca, *Chin. J. Anal. Chem.* **2015**, *43*, 983–988.

Manuscript received: April 10, 2024
Accepted manuscript online: June 3, 2024
Version of record online: July 17, 2024

© 2024 The Authors. Angewandte Chemie International Edition published by Wiley-VCH GmbH

15213773, 2024, 34, Downloaded from https://onlinelibrary.wiley.com/doi/10.1002/anie.202406867 by Ohio State University, Wiley Online Library on [12/08/2024]. See the Terms and Conditions (https://onlinelibrary.wiley.com/terms-and-conditions) on Wiley Online Library for rules of use; OA articles are governed by the applicable Creative Commons License